

Implication of palladium geometric and electronic structures to hydrogen activation on bulk surfaces and clusters

Irena Efremenko*

Wolfson Department of Chemical Engineering, Technion Israel Institute of Technology, Haifa 32000, Israel

Abstract

A great body of theoretical results obtained preferentially with density-functional methods in the last decade is analyzed with emphasis on the relationship between the orientation of the surface for semiinfinite mono-metallic bulk palladium and the cluster-size for finite palladium particles. It is demonstrated that the crystallographic orientation of a surface influences the local electronic structure and the geometric configuration of catalytic centers and this way changes their catalytic properties. Weakly bound molecularly adsorbed states and atomic adsorbates in the most reactive low-coordinated positions are especially sensitive to such changes. The unique feature of small palladium clusters, their ground state magnetism affects mainly the dynamics of dissociative adsorption and leads to the stabilization of pre-dissociated forms of adsorbate. © 2001 Elsevier Science B.V. All rights reserved.

Keywords: Palladium; Hydrogen; Quantum mechanics; Surface structure; Electronic structure of clusters

1. Introduction

The role of the structural factors in catalysis has been discussed for a long time and was especially underlined in the Balandin's multiplet theory in 1929 [1–4]. Even earlier the Taylor's assumption that the unsaturated metal atoms on edges and corners are especially active centers in surface reactions [5,6], is up to now the most common “geometric” hypothesis in catalysis. Whereas changes in the catalyst electronic structure along the rows and across the periods in the Periodic system, as well as alterations in electronic structure caused by supports, promoters and adsorbates, and their influence on surface chemistry and catalysis are widely discussed in the modern literature, relatively little attention is paid to the structural parameters such as the surface and bulk geometry and the particle size. Palladium — one of the best studied

catalysts with “magic” catalytic properties is a very convenient object for an analysis of the current state in understanding of the geometric factors in catalysis. For the explanation of the versatility of palladium in catalytic reactions, chemists widely used speculations based on assigning different roles to various surface centers with different geometries [7]. In spite of the great progress in experimental techniques applied for investigation of catalytic reactions and surface phenomena, molecular details of the structure and performance of such surface centers in elemental stages of a catalytic reaction may not be fully resolved from experimental data. In particular cases of hydrogenation and oxidation reactions, experimental investigations are hampered by an adsorbent penetration into the solid, leading to deformation of catalyst bulk and surface structure. Additional problems related to the bulk and surface geometry evolve in the case of such perspective catalysts as palladium nano-clusters. An experimental investigation of their structure and transformations under catalytic conditions is very complex,

* Fax: +972-4-8230476.

E-mail address: chirena@tx.technion.ac.il (I. Efremenko).

if not impossible. The possibilities offered by the modern quantum chemical techniques and computational resources should significantly complement the experiments in this area.

The catalytic function of palladium have been a focus of simulation efforts over many years starting from the earlier works of Baetzold [8–10]. The importance of such investigations stems from the wide application of different palladium catalysts in numerous reactions and from the great body of information gathered in experimental investigations, which have to be systemized and explained at the molecular level. Moreover, palladium is of special interest for the theoretical chemistry due to its special position in the Periodic system, it is the only element with $d^{10}s^0p^0$ electronic configuration. This electronic configuration of palladium atom changes in various situations depending on its chemical bonding and determines its specific chemical behavior. Hydrogen activation and surface chemistry have served as a classical model for understanding the mechanism of catalytic action in the vast majority of the basic research. The palladium–hydrogen system is one of the best studied from both the experimental and theoretical points of view. The extensive interest in hydrogen interaction with palladium surfaces is due to wide applications of this system in processes ranging from catalytic hydrogenation and fuel cells to energy storage and hydrogen purification. Theoretically, it is a well-suited model system for investigation of different aspects relevant to catalysis, since the palladium–hydrogen interaction exhibits a wide spectrum of fundamentally interesting topics, such as molecular and atomic adsorption and desorption, dissociation, indirect interaction between adatoms and formation of ordered superstructures, adsorbate-induced surface reconstruction, penetration into the bulk and phase transition. All these processes depend sensitively on the crystallographic structure of the surface.

In the foreword to the 1991 thematic issue of Chemical Reviews on Theoretical Chemistry, Ernst R. Davidson wrote, “The theory of transition-metal chemistry has lagged behind the quantum theory of organic chemistry because quantitative wave functions are more complicated” [11]. However, the first article in this issue [12] determined the direction for the future development in the theoretical transition-metal chemistry: the overwhelming innovation was the

widespread acceptance of density-functional theory (DFT) in the last decade in calculating transition-metal clusters and surfaces [13–15] along with dramatic progress in computer technologies. Although, the theoretical investigation of palladium catalysts and their interactions with hydrogen reflected the evolution in quantum chemical techniques for all the years, these latest achievements imply that a great number of high-level studies are devoted to the “hottest” aspects of palladium catalytic function. In the present review the progress made in the past decade towards an understanding of the electronic nature of hydrogen adsorption and activation on mono-metallic single crystal palladium surfaces and clusters will be discussed with emphasis on the relationship between surface structure and particle size, on the one hand, and catalytic properties on the other hand. The theoretical studies in palladium molecular chemistry and some important aspects of homogeneous catalysis by palladium complexes were reviewed recently [16] and will not be considered here.

In 1929, after the discovery of quantum mechanics, Dirac claimed: “The underlying physical laws necessary for the mathematical theory of a large part of physics and the whole of chemistry are thus completely known, and the difficulty is only that the exact application of these laws leads to equations much too complicated to be soluble” [17]. Really, for randomly placed nuclei and defined number of electrons, solving the Schrödinger equation one can get electronic configurations, which correspond to the lowest and excited states of the system for a given configuration. Minimizing energy with respect to the nuclear positions one can find the geometry, which corresponds to the lowest energy of the system (ground state), or to local minima (i.e. conformers). Thus, the following aim of quantum chemistry is to find the best approximation for the Schrödinger equation and to apply it to the best model describing the system in hand. Let us consider briefly the current methods and models used in quantum chemical applications for the heterogeneous catalysis and surface phenomena, in order to provide a reader unfamiliar with modern quantum chemistry with the ability of different approaches and with the main notations used in the following discussion. Neither the underlying theoretical background nor mathematical treatment will be considered here. This information can be found in innumerable reviews

and books on conventional quantum mechanics (see, for example [18–21]) and DFT [13–15,22–26], including those devoted to quantum chemical approaches to catalysis [27,28].

2. Methodological remarks

2.1. Methods

Depending on the main concept of approximation, electronic structure methods may be divided into three distinct classes: ab initio, density-functional and semiempirical methods. For a long time the Hartree–Fock self-consistent field (HF-SCF) approach, based on the assumption, has been the most developed, theoretically the most rigorous and practically the most applied. In this approximation molecular orbitals (MO) are constructed by linear combination of atomic orbitals (LCAO), also called basis functions. Each AO may be presented by a single orbital (minimal basis) or splitted into two (double- ζ , DZ) or more orbitals, in order to make a basis set more flexible. For very heavy elements, the kinetic energy of the electrons in the region immediately surrounding the nucleus is very high (the speed of the electrons in the innermost core orbitals for nucleus $n = 50$ is about one-half of the velocity of light). Therefore, for such electrons the effects of relativity must be accounted for. Since the primary concern for quantum chemists is the behavior of valence electrons, and the deeper core electrons of very heavy atoms do not change significantly in a molecular environment, core electrons are often replaced by an effective core potential (ECP), in which relativistic effects (RECP) can be automatically included [29–31].

In its original form HF approximation does not properly account for electron correlation, and simple HF-SCF approach is known to yield poor geometries and energetics, especially for transition-metal containing systems. In order to improve the situation, configuration interaction (CI) post-HF multiconfigurational SCF (MCSCF) methods were developed. The simplest and most applied of them is the second-order Møller–Plesset perturbation theory (MP2). Another methods that vary the initial one-electron functions and expand the many-electron wave function to incorporate a more complete representation of the active space are based on the self-consistent treatment. The level of correlation treatment and the extend of the

completeness of the set of basis functions determine the accuracy of HF calculations; in the limit of full correlation interaction and complete basis set the method should lead to exact solution of the (non-relativistic) Schrödinger equation [32]. The main drawback of the method is that computing time and disk storage requirements scale as n^4 for HF and n^7 for post-HF calculations (where n is the number of basis functions). Thus, for large transition-metal systems, a full CI expansion is computationally inconceivable at the present time. The results of accurate ab initio calculations are available for palladium systems with not more than five metal atoms.

The more recent and perspective approach is that of the density-functional theory (DFT) [13–15,22–26] based on the theorems of Hohenberg and Kohn [33]. The inherent advantage of DFT is that the total electronic energy is directly tied to electron density. Each electron is considered as moving in the effective local potential of nuclei and other electrons (Kohn–Sham orbitals) [34], and therefore, the electron interactions are treated explicitly as a function of density. This reduces the computational burden of treating intensive and cumbersome electron–electron terms; DFT methods scale as n^3 . Since DFT included corrections to HF energies for correlation energy, the structures and relative energies became much more reliable — the accuracy of DFT methods is comparable with that of rigorous ab initio CI methods (usually at MP2 level). Basis sets for DFT calculations, including the most popular small-core RECP basis sets, have been rigorously optimized and can in many cases provide better solutions than their ab initio counterparts due to a better representation of the unfilled valence orbitals. The other advantage of DFT is that it provides some chemically important concepts, such as electronegativity (chemical potential), hardness (softness), Fukui function, response function, etc. These calculations also make it possible to analyze the electronic structure of molecules with the aim of gaining insight into the chemical bond and deriving bonding models, which can be compared with the existing models of chemical bonding [35–39]. Here, DFT again has proven to be very powerful, because the Kohn–Sham orbitals turned out to be even more helpful for a bonding analysis in terms of orbital interactions than the Hartree–Fock orbitals, since the former include correlation effects.

The main disadvantage of the DFT is that the exact form of the exchange–correlation functional is unknown and one should use approximate potentials. There is no such a systematic way in DFT to improve its results as in the conventional *ab initio* theory; in this sense DFT is not strictly the first principle method. Nevertheless, recent progress in DFT has shown clearly that the new generation of gradient-corrected DFT methods such as the Becke's three-parameter hybrid exchange potential (B3) [40–42] with the Lee–Yang–Parr (LYP) correlation functionals [43], local density approximation (LDA) and more recent general gradient approximation (GGA) [44,45] are efficient and accurate computational methods in the studies of reactions on transition metal surfaces. The LDA results for bond dissociation energies have an overbinding tendency. The inclusion of gradient corrections to DFT provides bond dissociation energies, which pair in accuracy with MP4 results. DFT is a method of choice for transition states and vibrational frequencies in transition-metal containing systems, again the inclusion of gradient corrections improve an agreement with experiment. The hybrid B3PW91 and B3LYP functionals used with extended basis sets and relativistic ECP were shown to provide excellent results for the singlet–triplet separation energy of palladium atom [46].

Semiempirical methods, i.e. those in which some integrals are replaced by empirical parameters, are currently applied for very large systems. In these methods only valence electrons are usually considered. Semiempirical calculations are faster than the typical *ab initio* or DFT calculations by at least three order of magnitude [47], but are generally less accurate. The relatively sophisticated group of semiempirical MO LCAO methods, in which the electron repulsion is treated at various levels of accuracy, is constituted by neglect of differential overlap (NDO) methods [48–50] (CNDO, MINDO, MNDO, AM1, PM3, etc.). The parameters for transition-metal complexes are developed now within several of these methods [51–53]; however, the inherent features of the NDO approximation limit their application for transition metal surfaces and catalysis. The main of these features are large number of parameters that have to be optimized, poor representation of hypervalent, excited and transition states and π -complexes, and the strong dependence on proper parametrization.

These methods are parametrized and thus, perform better for transition-metal complexes but not for sterically unusual molecules [54], as in the case of surface ensembles. Moreover, interpreting the orbitals from NDO methods leads to some difficulties, since they often give a very poor approximation for the wave function.

In the extended Hückel theory (EHT) methods, the electron repulsion integrals as well as core–core interactions are not included at all. In this sense, EHT is the simplest MO LCAO method. The strong point of the EHT is that the orbital overlap in this method is treated in the explicit form, therefore, it enables to take into account the principal interactions between basis orbitals and to imagine the shape of resulting MO [55]. It is proven now that DFT, HF and EHT methods usually predict similar shape, symmetry properties and energy order of the occupied orbitals [56]. The EHT approximation is more easily derived from the DFT than from *ab initio* quantum chemistry, as the justification of both DFT and EHT models has a common key [57,58]. The empirical parameters for EHT calculations have a well-defined physical meaning and are available for all the elements in Periodic table. The simple techniques based on the EHT treatment [59] have made important contribution towards understanding various catalytic chemistries through the reaction mode analysis of the surface chemistry in the terms of detailed orbital interactions. An extension of the EHT approach, that empirically accounts for repulsive interactions, was introduced in the atomic superposition and electron delocalization molecular orbital (ASED MO) method [60–62]. This improvement was aimed at obtaining more reliable values of the total energy and at gaining an opportunity to optimize the geometry of chemisorption structures. Comparing with NDO methods, the ASED MO better describes the geometry of reactive complexes and the bond cleavage in catalytic processes [63]. The ASED MO theory has been extensively applied to the catalytic and electrochemical processes occurring on surfaces of metals and oxides [60–62,64–69].

Several semiempirical techniques were developed strictly for the analysis of extended metal systems. Among them are the tight-binding method (TB) [70–72] of essentially Hückel type, the effective medium theory [73] and the related embedded-atom method (EAM) [74], in which the atomic electron den-

sity is manipulated to handle the effects of embedding into an extended lattice. These methods are useful for situations in which quantum mechanical effects are significant, but the system size makes *ab initio* calculations impractical. Efforts continue to be mounted in order to improve existing semiempirical methods. Probably, the most promising is the *ab initio* TB model, which is very similar to the Kohn–Sham method [75].

Much progress has been made in the recent years in the theoretical description of surface reactions by high-dimensional dynamics simulations on potential energy surfaces, which are derived from high-level total energy calculations [76]. That provides a more direct link between what experimental studies observe and what theory predicts. The bond order conservation methods [77,78] for determining metal surface reaction energetic, which significantly contributed to understanding of catalytic reaction mechanisms, are often applied in conjunction with the high-level quantum chemical methods.

2.2. Models

The application of the theory to the heterogeneous catalysis is characterized by two clearly defined model approaches. Historically, the first local approach consists of the consideration of the interactions of the adsorbed molecules only with the nearest atoms of the surface of a catalyst. Key importance is ascribed in this case to the defects and various imperfections of the crystal lattice at the solid surface. A relatively small fragment known as a cluster simulates an active catalytic site in this case. The numerous quantum chemical computations carried out for such clusters have demonstrated that chemisorption interactions are indeed sufficiently localized, even in the case of metals, where maximal cooperative effects should be anticipated. This conclusion is also in accordance with the rich chemical experience such as the close analogy between the homogeneous and heterogeneous catalysis, the data on the chemisorption and catalysis on alloys, a number of various spectral and physicochemical methods, and so on. The main shortcomings of this model are: (i) relatively small size of the model cluster, which may be treated at high theoretical level; (ii) dangling bonds on the boundary of a cluster, which lead to unreasonable distribution of the

electron density; (iii) low convergence of calculated energies with the cluster-size; and (iv) convergence problems, which arise from a large number of nearly degenerated states, typical for transition-metal systems, and from an unreasonable electron density distribution on the boundary of the cluster [79–81].

In the opposite approach a catalyst is considered as an infinite periodic slab, where electrons can be transferred over considerably large distances. The chemisorption and chemical activation of adsorbed molecules in such a system are treated by taking into account the symmetry of regular crystal lattice and the ability of free electrons or holes to be localized within the adsorption region. This collective approach originates from the band theory of the electron structure of solids and it is physically more reasonable. However, some disadvantages arise from the periodicity: (i) modeling of surface defects and irregularities, which are usually very important in the surface chemistry and catalysis, requires an employment of a very large supercell that leads to the substantial increase in the computational burden; (ii) only relatively high and well-organized coverages may be modeled, that is especially inadequate for modeling of elementary chemical act; (iii) it is difficult to model changes in a substrate geometry along a reaction pathway, especially in the surface plane. Probably, the periodic approximation performs better for calculations of the accurate geometry and energetics of lengthy surfaces in the ground state, while the cluster approximation allows one deeper insight into the structure and nature of the transition states and potential energy surfaces (PES).

The main conclusions from the above remarks may be formulated as follows. While 10 years ago it was correct to say that all kinds of quantum chemical methods are applied for surface phenomena and catalysis, today computational transition metal chemistry is almost synonymous with DFT. The most accurate methods can predict energetic properties of transition-metal systems to within 5–10 kcal/mol. This level of accuracy enables the dynamic of surface reactions to be effectively modeled. Semiempirical methods continue to have an important role in providing the concepts and language of chemistry. In this content the simplest of these methods may be more important than the most complicated [82]. From such calculations much can be learned to guide and formulate critical experiments

in the design of new catalysts. The cluster approximations seem to give way to those based on the periodic boundary conditions, which, in line with other advantages, are computationally more effective due to the more realistic wavefunctions.

The topics of the account below are the quantum chemical studies using the DFT and ab initio methods, which focus on the analysis of the chemical properties on and within palladium surfaces and clusters and their transformations during surface processes. Works that are based on the EHT calculations and earlier theoretical studies will only be discussed if it is relevant in the context of recent accurate studies. For the bulk palladium surfaces, the slab model results will be examined first; cluster model calculations will be considered to complement these data.

3. Geometric and electronic structures of bulk palladium surfaces

In this section the geometry, energetics and electronic structure of the three low-index palladium crystal faces (111), (100) and (110) will be

briefly considered. Even though the local nature of catalyst–adsorbent interaction is generally accepted, bulk transition-metal catalysts show two main differences when compared with homogeneous catalysts: a large number of electrons on nearly degenerated orbitals in overlapping d-, s-, and p-bands and a significantly higher coordination number of metal atoms. The structure of three low-index surfaces of fcc palladium are shown in Fig. 1. While each palladium atom in the bulk has 12 nearest neighbors, at the (111), (100) and (111) surfaces 3, 4 and 5 neighbors are absent. Once Pd atom forms chemical bonds, its closed-shell electronic configuration is perturbed and a part of electron density is moved from 4d AOs to 5s and 5p orbitals. Table 1 demonstrates how the orbital occupations and the bond populations of a surface palladium atom depend on the structure of the palladium surfaces shown in Fig. 1. One can see that the more open is the surface, the smaller is the perturbation in the electronic structure of the palladium atom and the less electronic density is shared for Pd–Pd bonding. This determines variations in the geometric structure, magnetic properties, work function, surface energy, bands structure and reactivity of the surfaces. Let us

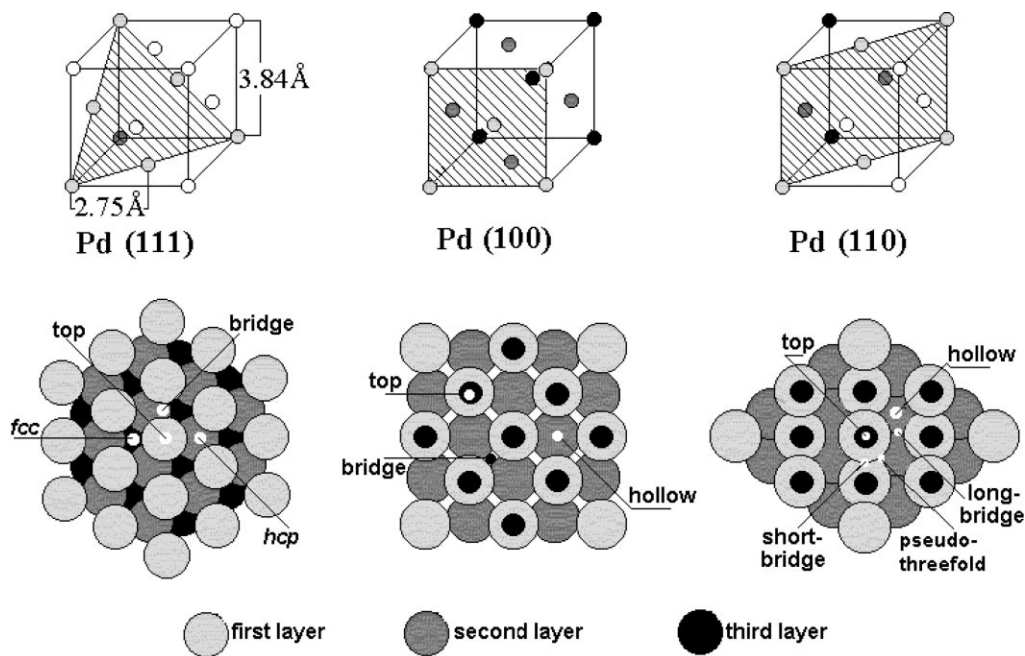


Fig. 1. Schematic representation of the close packed fcc palladium surfaces and highly symmetric adsorption sites on them.

Table 1
Mulliken population analysis for bulk and surface palladium atoms on different crystal faces (EHT calculations)

Surface	Orbital occupations			Bond populations				
	5s	5p	4d	Bond in surface layer	Total in surface layer	Bond first–second layer	Total first–second layer	Total per Pd atom
Bulk	0.136	0.118	9.754					0.516
Pd(1 1 1)	0.107	0.089	9.802	0.046	0.276	0.043	0.129	0.405
Pd(1 0 0)	0.098	0.082	9.816	0.050	0.200	0.043	0.172	0.372
Pd(1 1 0)	0.090	0.072	9.835	0.049	0.098	0.047	0.188	0.286

consider briefly some of these properties relevant to surface chemistry and catalysis. The corresponding computational results are summarized in Table 2, in comparison with the available experimental data.

All the surfaces tend to change their geometric structure in order to reduce the surface energy and to maximize the surface coordination. Two main types of changes are the surface relaxation (usually, contraction between the first and second layers) and the surface reconstruction, accompanied by the movement of surface atoms and formation of close packed overlayers. The direction and level of transformations are determined by the relationship between an energetic benefit granted by the new or contracted bonds and energy losses associated with the break and deformation of other bonds. If the energy of the system is not high enough to overcome an activation barrier for reconstruction, the metastable configuration may be preserved. Periodic LDA calculations with ultrasoft potential [92] indicate that the relaxation of the compact Pd(1 1 1) surface is very small, while more recent GGA calculations [93] show a

notable relaxation that does not fully agree with the experimental data [94,95]. For Pd(1 0 0) face, the DFT results [96,97] indicate a slight inward relaxation of the topmost layer while the deeper layers show no relaxation. That again is inconsistent with the LEED data [98]. The substantial outward relaxation for Pd(1 0 0), attributed to the structure of the density of states near the Fermi level, was obtained in the classical TB scheme [99]. The most pronounced surface relaxation exhibits the crystallographically “open” Pd(1 1 0) face [100], in good agreement with the LEED structure analysis [101,102]. While (1 1 0) surfaces of transition-metals at the end of 5d series show the missing row (MR) reconstruction, for the clean Pd(1 1 0) surface no spontaneous reconstruction was found, but the non-reconstructed structure is only 5 [100] to 20 [103] meV per unit cell more stable than the MR structure. This is well consistent with the experimental observations of the step formation [104] and of the conservation of oxygen-induced reconstruction after the adsorbent elimination [105].

Table 2
Calculated and experimental characteristics of low-index palladium surfaces: relaxation of the first (Δ_{12}) and second (Δ_{23}) layers, work function (φ), surface level shift for d orbitals ($\delta\epsilon_{id}$) and surface energy (σ)

	Method	Pd(1 1 1)	Pd(1 0 0)	Pd(1 1 0)
Δ_{12} , %	GGA	−0.44 [93]	−0.6 [97]	−8.6 [100]
Δ_{23} , %	GGA	+0.32 [93]	~0.0 [97]	+3.7 [100]
Δ_{12} , %	Experimental	−1 ± 2.5 [94]; −1.1 ± 2.2 [95]	+3 [98]	−5.1 ± 1.5 [101,102]
Δ_{23} , %	Experimental	−3.5 ± 1.3 [94]; 0.0 ± 2.2 [95]	−1 [98]	+2.9 ± 1.5 [101,102]
φ , eV	GGA	5.75 [83]	5.38 [108]	4.85 [103]; 4.90 [159]
φ , eV	Experimental	5.44–5.55 [84–86]	5.22–5.8 [87–89]	
$\delta\epsilon_{id}$, eV	LDA	0.38 [90]	0.54 [90]	0.63 [90]
σ , eV/atom	GGA		0.49 [152]	1.09 [100]
σ , eV/atom	LDA	0.824 [91]	1.152 [91]	1.559 [91]
σ , J/m ²	LDA	1.920 [91]	2.326 [91]	2.225 [91]

As authors [98] suggested, the discrepancy in the surface geometry between experimental and theoretical studies may be attributed to the surface ferromagnetism. Indeed, in the magnetic state, the electronic density from the Pd 4d orbital is transferred to Pd 5s AOs that makes interatomic interaction stronger. The bulk palladium has a very large magnetic susceptibility, even though it is non-magnetic at the equilibrium lattice constant. For a lattice expansion of only 3% (4.0 Å) a small magnetic moment appears, which increases abruptly up to a value of 0.36 μ_B per atom for an 11% expansion (lattice parameter of ~ 4.3 Å), after which it saturates [106,107]. The recent DFT [108] and TB [109] calculations of magnetic properties of Pd(100) surface show very interesting results: it appears that calculated magnetic moment on the surface layer depends on the thickness of the slab, but it is always smaller than that at the deeper layers.

The calculated work functions (Table 2) show a strong dependence on the surface morphology and agree well with the measured values. Increasing of the highest occupied level for more “open” surfaces is supported by the calculated surface level shift for 4d orbitals. The surface energy, as a measure of bonding at the surface, reflects increasing coordination unsaturation when moving from Pd(111) to (100) and to (110) faces. Besides of the above mentioned differences, the geometric structure of coordination sites available for interaction with adsorbate differs on distinct crystal faces.

4. Interaction of an atomic hydrogen with palladium surfaces

Numerous theoretical studies devoted to the hydrogen adsorption on palladium range from simple conceptual to sophisticated numerical. The main objectives of these studies are: (i) the determination of the most stable adsorption site and the nature of the bond between hydrogen atoms and different coordination sites on palladium surfaces; (ii) the adsorbent-induced changes in the geometric and electronic structures of the catalyst; (iii) the hydrogen ability to penetrate a surface as a first step of its dissolution in bulk; and (iv) the inquiry into the dissociative interaction of H₂ molecule with Pd catalytic centers.

Experimentally, the interaction of hydrogen with the single crystal and polycrystalline palladium surfaces has been studied by means of thermal desorption spectrometry (TDS) [110–117], LEED [114,118–121], surface-potential change measurements [104,114–116,120,122], He diffraction [123], electron energy loss spectroscopy [124], low-energy ion-scattering spectroscopy [125], IR [126,127], photoemission [128], UV [129–134] and kinetic [135] methods. These results demonstrate that, in addition to the hydrogen absorbed in the bulk palladium, there are various forms of activated hydrogen bound to the catalytic surface by a unique manner and showing unlike chemical behavior. Several important experimental characteristics of the hydrogen adsorption on palladium single crystal surfaces are presented in Table 3, together with the calculated results for the ground state hydrogen adsorption at coverage $\theta = 1$. The surface hydrogen patterns were found to have a diminutive positive [136,137,122] or negative [114,117] charge. While relatively little differences in the adsorption properties of the Pd single crystal planes were observed, the reactivity [138–141] and selectivity [142,143] of the adsorbed hydrogen strongly depend on the surface structure.

4.1. Geometry and energetics of high-symmetry coordination sites

Theoretical studies of atomic hydrogen adsorption on the low-index palladium surfaces and its penetration into the near-surface region and dissolution in the bulk were conducted by DFT and semiempirical methods using both cluster and periodic models. Bond distances obtained in the cluster calculations are consistent with those from the periodic calculations and with the experimental results. However, the energetics of hydrogen–palladium interaction and even the preferential location of hydrogen atom depend on the cluster size [145–148,322] and usually are in poorer agreement with the experimental data than the corresponding results of periodic calculations. One of the possible reasons for such disagreement is that in the cluster calculations very low coverages (actually, zero-coverage limit) are treated, as opposed to experimental conditions. However, a detailed analysis of the orbital populations in hydrogenated palladium clusters shows that the adsorbent-induced alterations in the

Table 3

Experimental and theoretical characteristics of an atomic hydrogen adsorption on low-index palladium surfaces: initial heat of H₂ adsorption (Q), temperature of the main thermodesorption peak ($T_{des.}$), maximal work function increase ($\Delta\phi$), the most stable adsorption position, calculated adsorption energy (AE) with respect to H₂ molecule (for comparison with Q) and Pd–H bond length (d_{Pd-H}) for this position and activation energy for H-atom surface diffusion ($E_{dif.}^\ddagger$)

	Method	Pd(111)	Pd(100)	Pd(110)
Q , eV	Experimental [114,120,115]	0.90	1.06	1.06
$T_{des.}$, K	Experimental [114,120]	390	360	350
d_{Pd-H} , Å	Experimental [95,144,119]	1.78	1.97 ± 0.1	2.0 ± 0.1
$\Delta\phi$, eV	Experimental [114,120]	0.18	0.20	0.36
Stable position	GGA [159]	fcc	Hollow	Pseudo-three-fold
AE, eV		1.02	1.04	1.00
d_{Pd-H} , Å		1.82	1.99	1.81; 1.81; 1.83
$E_{dif.}^\ddagger$, eV		0.19	0.12	0.11 ^a ; 0.10 ^b

^aFor surface diffusion perpendicular to {110} rows.

^bFor surface diffusion along {110} rows.

Pd–Pd bond strength contribute significantly to the resulting hydrogen adsorption energy and in particular, determine the energetic differences between adsorption sites with the same coordination number on different crystal faces [148]. In order to account for such alterations the size of model cluster should be very large, far beyond the size that may be treated by high-level methods. Thus, the most important source of error has to be attributed to the inherent disadvantage of the cluster model. Therefore, here we will concentrate on the DFT results obtained with slab calculations.

An atomic hydrogen adsorption on the Pd(111) [92,149–151], Pd(100) [152–159] and Pd(110) [103,152,160,161] surfaces at coverages $\theta = 0.25$ –1, 0.25–2 and 0.5–1.5 monolayer (ML), respectively, was studied using LDA and GGA approximations with frozen or relaxed slab models. The comparative theoretical study of the coordination sites with a similar geometry on and just below the three low-index palladium surfaces at full coverage ($\theta = 1$) was performed by Dong et. al. [159] within GGA approximation with optimized ultrasoft pseudo-potentials and five, eight and nine slab models for the (111), (100) and (110) surfaces, respectively. Although, numerical results obtained with different approximations, basis sets and models are slightly different, the main features of the palladium–hydrogen interactions agree closely with each other. Thus, our comparison of the coordination sites for hydrogen capping on/below the three surfaces will be based

mainly on the results of this last work. As one can see from Table 3, the computational results for the most stable adsorption positions agree nicely with the experimental measurements. Calculated data on the geometry, adsorption energy and several electronic properties for hydrogen adsorption/absorption in the high-symmetry sites on/below the low-index palladium surfaces are summarized in Table 4.

Analysis of the presented data show that the most stable hydrogen adsorption corresponds to the surface coordination with the largest coordination number; the subsurface absorption is less stable than surface adsorption and one-fold top coordination is energetically unfavorable. Calculated adsorption energy for the most stable sites is little affected by the surface orientation. Due to the saturation of dangling surface bonds, the adsorption of a ML of hydrogen on the Pd(111) and (100) surfaces changes the inward relaxation of the top layer of the clean substrate into an outward relaxation. The large inward relaxation of the topmost layer of clean Pd(110) surface decreases significantly under the hydrogen adsorption and for all coordination positions, except of long bridge one, is accompanied by a decrease in outward relaxation of the next layer. The bridge positions correspond to the transition state for the surface diffusion on the Pd(111) and (100). On the Pd(110) the short bridge site and the low-symmetry position in-between the pseudo-three-fold and the long bridge sites determine the activation barriers for surface diffusion perpendicular and along {110} rows, respectively; contrary to

Table 4

Adsorption energies per hydrogen atom, calculated with respect to half the experimental energy of the hydrogen molecule (E_{ad} , eV), distance of the adsorption site from the next substrate surface (subsurface) atom ($d_{\text{Pd-H}}$, Å), Mulliken charges on an adsorbed hydrogen atom (q , e^-), changes in the work function ($\Delta\phi$) and relaxation of the first (Δ_{12} , %) and second (Δ_{23} , %) substrate layers (All data from Ref. [159], except as otherwise noted)

Pd(1 1 1)	fcc	hcp	Bridge		Top	OSS
E_{ad}	0.51	0.45	0.32		-0.04	0.19
$d_{\text{Pd-H}}$	1.82	1.82	1.73		1.55	1.95
q [149]	-0.1	0.0	-0.1		+0.25	-0.3
Δ_{12}	+1.9	+3.3	+2.3		+2.7	+7.0
	Relaxation of the clean surface Δ_{12}			0.1		
Pd(1 0 0)	Hollow		Bridge		Top	OSS
E_{ad}	0.52		0.40		-0.08	0.18
$d_{\text{Pd-H}}$	1.99		1.72		1.55	1.93 (2.02)
$\Delta\phi$ [97]	+0.18		+0.39		+0.18	-0.19
Δ_{12}	+4.4		+1.9		+2.7	+8.8
	Relaxation of the clean surface Δ_{12}			1.0		
Pd(1 1 0)	PTF ^a	LB ^a	SB ^a	Hollow	Top	OSS
E_{ad}	0.50	0.43	0.39	0.18	-0.07	0.20
$d_{\text{Pd-H}}$	1.81 (1.83)	1.98 (1.88)	1.72	2.44 (1.63)	1.55	1.82 (2.00)
$\Delta\phi$ [103]	+0.15	+0.07				
Δ_{12}	-1.6	-4.4	-2.3	-1.7	-7.1	+5.1
Δ_{23}	+2.4	+4.5	+2.7	+2.6	+3.2	+4.8
	Relaxation of the clean surface Δ_{12}					-8.6
	Relaxation of the clean surface Δ_{23}					+3.7

^aPTF: pseudo-three-fold, LB: long bridge, SB: short bridge positions.

expectations both activation barriers appear to be very similar (see Table 3). The diffusion barrier is strongly dependent on the lattice constant. If the lattice constant of bulk palladium ($a_0 = 3.91 \text{ \AA}$) is used, the barrier height is twice as large as that for the equilibrium lattice constant of the palladium hydride β -phase ($a_0 = 4.07 \text{ \AA}$) [162]. From the subsurface positions, the octahedral site (OSS) (located on the Pd(1 1 1) surface just below the fcc surface position) is more stable than the tetrahedral one (TSS) (located below the hcp position). In the tetrahedral vacancy the optimized position of a hydrogen atom is close to the center of the Pd₄ tetrahedron, while in the octahedral position hydrogen moves out of the geometric center towards the topmost layer.

For the three-fold coordination on Pd(1 1 1) and pseudo-three-fold coordination on Pd(1 1 0) the Pd-H bond lengths are very similar, while on the Pd(1 0 0) surface there are four longer Pd-H bonds. For other surface sites the similarities in the adsorption geometries are even more remarkable while the adsorption energies differ significantly, especially for the two-fold

coordination. The atomic charges on hydrogen atoms and Pd-H bond occupations reflect generally the adsorption geometries and are very similar for similar coordination complexes on different crystal faces [148]. These data indicate rather local bonding character of hydrogen adsorption. The energetic differences for similar coordination positions on different crystal faces arise from the hydrogen-induced changes in the interatomic bonds between nearest palladium atoms. Such changes are rather small in absolute value but they have relatively distant nature and extend up to the next-neighboring to the hydrogen-bound metal atoms in both parallel and perpendicular to the surface direction. This effect is, probably, of general nature in adsorption of various adsorbates on metal surfaces. Thus, the local nature of adsorbent-surface interaction can underlie the experimentally observed small dependence of adsorption heats on the surface structure, whereas the distant nature of electronic perturbations in the adsorbate should define the correlation between an adsorption energy and a coordination number of surface atoms [163].

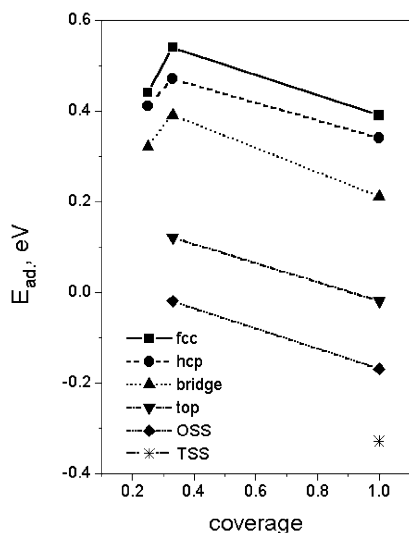


Fig. 2. Coverage dependence and relative stability of the surface (fcc, hcp, bridge and top) and subsurface octahedral (OSS) and tetrahedral (TSS) sites for hydrogen coordination on/below the Pd(111) surface (derived from the data of [151]).

Fig. 2 shows the coverage dependencies and relative stability of the surface (fcc, hcp, bridge and top) and subsurface OSS and TSS sites for hydrogen coordination on/below Pd(111) surface at submonolayer coverages. The coverage dependencies have an extremal character. At coverages $\theta \geq 0.4$ the adsorption energy increases with decreasing hydrogen concentration due to the repulsive interaction between hydrogen atoms. At lower hydrogen loadings the weakness of hydrogen adsorption with decreasing coverage indicates an indirect attractive interaction between nearest neighbor hydrogen atoms and implies the island formations for low coverages. On the Pd(100) surface the similar maximum of E_{ad} was obtained at $\theta = 0.5$. The stability of the bridge position was found to decrease with decreasing coverage on this surface. As the energetic difference between hollow and bridge positions determines the diffusion barrier height, it causes the increase of activation energy for hydrogen surface diffusion that again favors the island formation at low coverages. Due to the computational difficulties in modeling of low-symmetry surface arrangements the geometric and electronic structures of such islands are poorly known yet. The optimized geometries of the adsorbed hydrogen are less dependent on the cov-

erage, while the TB calculations [164] show that the surface relaxation is strongly coverage-dependent.

4.2. Surface reconstruction

The crystallographically “open” (110) surface shows the most pronounced hydrogen-induced changes in the geometry of the topmost and several next layers. While clean Pd(110) surface shows no reconstruction, hydrogen adsorption induces two types of reconstruction: pairing-row (PR) and missing row (MR). The former type of reconstruction represents paired surface movement of {110} rows to one another, while the latter is connected with pushing of some inner layer rows above the surface with formation of (111) facets. Both types of reconstruction were observed [115,116,118,165–170] and calculated [160,161] to be a strong function of hydrogen concentration and temperature. For submonolayer coverages two ordered structures of MR type were observed at 300–350 K [165] while at 200 K no surface reconstruction was found for $\theta \leq 1$. At higher hydrogen exposure the Pd(110) surface restructured into paired rows with the additional H-atoms sitting in-between. This structure is the most pronounced in the LEED at $\theta = 1.5$ and the temperature below 200 K. MR reconstruction appears at high hydrogen concentration at the temperature above 250 K [169,170]. Many other surface geometries were observed on the Pd(110) surface at higher temperatures. Although, the way in which the substrate reconstructs can be clearly deduced from experiments, the way in which H-atoms are arranged on the reconstructed surfaces is not so well established, since direct experimental observation of surface H-atoms is usually impossible.

Several theoretical studies were concentrated on hydrogen arrangement on unreconstructed and reconstructed Pd(110) surfaces as well as on fundamental theoretical issue of driving forces for the surface rearrangement [103,146,160,161]. A variety of models were studied in detail. Only particular arrangements of hydrogen atoms were shown to induce surface reconstruction, for other structures exertion forces bring the surface to the unreconstructed structure. Fig. 3a shows three possible structures, the PR, the MR and the unreconstructed phase containing hydrogen atoms in subsurface sites (SS), which are consistent with patterns experimentally observed at $\theta = 1.5$. In the PR

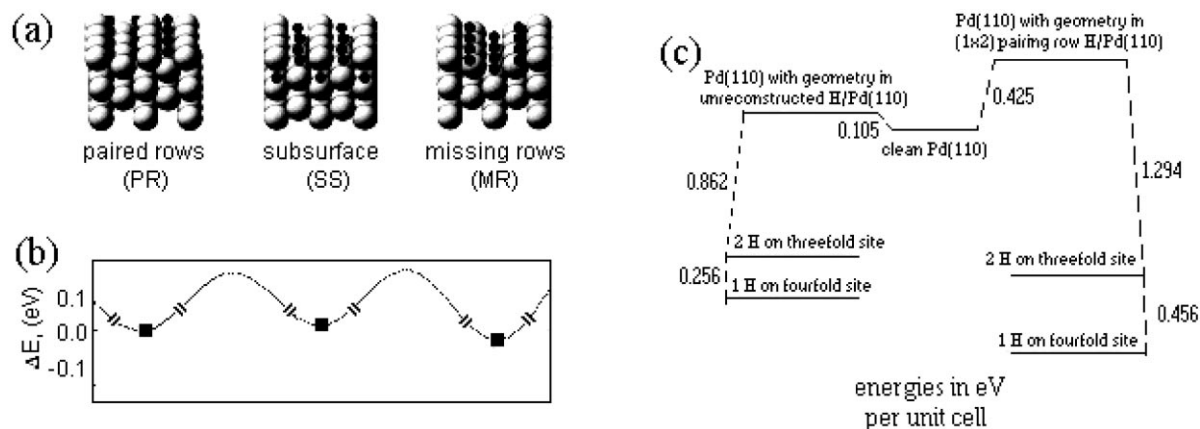


Fig. 3. Schematic view of the Pd(110)-(1 × 2) paired-row reconstructed surface (PR), the Pd(110)-(2 × 1) reconstructed surface with occupied subsurface sites (SS), and the Pd(110)-(1 × 2) MR reconstructed surface (MR) at hydrogen coverage $\theta = 1.5$ (a); schematic representation of their energetic differences ΔE_s and non-zero activation barriers for the mutual transformations (b). Reproduced with permission from D. Tománek, S. Wilke, M. Scheffler, Phys. Rev. Lett. 79 (1997) 1329. Top view of the PR surface and interaction energy decomposition analysis of the driving force for the pairing-row reconstruction (c). Adopted from [100].

and MR structures one ML of hydrogen is placed in pseudo-three-fold sites and the remaining 0.5 ML of hydrogen is in long-bridge sites of troughs. In the SS structure one ML of hydrogen is in bridge positions of troughs and the remaining 0.5 ML of hydrogen is in octahedral subsurface sites. These three structures were found to be energetically nearly degenerated (Fig. 3b) with the calculated surface energy differences within 0.06 eV [103]. This fact explains a large variety of coexisting surface arrangements observed experimentally, and activation barriers for their transitions (schematically shown in Fig. 3b) determine the temperature dependence of surface patterns. The driving forces for the PR surface reconstruction may be understood from the decomposition of the interaction energies shown in Fig. 3c. While the reconstruction of the Pd(110) surface itself gives increase in energy, it better interacts with hydrogen atoms in both pseudo-three-fold and hollow sites. Since each hydrogen atom on the surface accumulates an excess charge of 0.1–0.2 e⁻, the PR reconstruction is attributed to a gain in the Coulomb energy [103,160,161]. At $\theta = 1$ the MR reconstruction further increases the distance between hydrogen atoms sitting on the neighboring rows and gives energy gain of 0.059 eV [160,161]. Then additional 0.5 ML of hydrogen are placed in the pseudo-three-fold positions between the second and third layers, the resulting structure is by 0.04 eV more

stable than the PR configuration at the same coverage. The MR reconstruction appears to be energetically favorable even at the coverage as small as 0.5 ML. Thus, DFT calculations support the experimental observations that the MR reconstruction is more stable than the PR and unreconstructed configurations even at low hydrogen coverage, but its formation is hindered by an activation barrier owing to a large mass transport. The driving force for the MR reconstruction is ascribed to the better adsorbate–substrate interaction on the reconstructed surface [160,161].

4.3. Subsurface absorption

The ability of hydrogen to occupy subsurface positions is of particular interest as a first step in formation of α - and β -palladium hydride phases. The investigation of thermodesorption spectra revealed the formation of subsurface hydrogen within temperature interval 115–140 K at pressure as low as 10⁻⁴ Pa [117]. On the Pd(111) surface two ordered structures with $(\sqrt{3} \times \sqrt{3})R30^\circ$ symmetry were found experimentally for $\theta = 1/3$ and $2/3$ below the critical temperature of 85 and 105 K, respectively [171–173]. The best agreement between the LEED measurement and the dynamical LEED calculations was obtained for a mixing of surface fcc and subsurface octahedral sites with subsurface occupation fractions up to 60%. As

the temperature is raised, more hydrogen was found on the surface [174], and in the room-temperature experiments [175] hydrogen populated only the surface positions. Theoretically, occupation of the subsurface positions is ruled out for rigid metal structure and high coverage, however, hydrogen adsorption, and especially hydrogen absorption, induce a significant outward surface relaxation that makes the SS more stable [149]. The frozen structure of the close-packed Pd(111) surface hampers hydrogen penetration through the surface with activation barrier of 0.47 eV; allowing the surface interlayer spacing to relax modifies this value to 0.33 eV [149]. This situation corresponds to a simultaneous penetration of a 1×1 H array. At $\theta = 1/3$ in-plane relaxation becomes possible, and in this case hydrogen penetrates the surface without an activation barrier [151]. The experimentally observed structures with mixed population of surface and subsurface positions were reproduced by the embedded atom method combined with Monte Carlo simulations [176] and by TB [177] calculations. The simultaneous occupation of surface and SS in both ordered structures was attributed to the more attractive interactions between pairs of surface fcc and subsurface octahedral impurities, located in the nearest positions, in comparison with the lateral interactions.

The interest in high coverages considered for Pd(100)–H interactions was enhanced by the experimentally observed in the Pd(100)–H system saturation coverage $\theta \approx 1.35$ (at 170 K) [120]. For $\theta > 1$ there are two possible structures on this surface: with additional hydrogen incorporated below the surface and the island formation of the bridge-bound hydrogen with a local coverage $\theta = 2$. Although, the latter configuration is energetically possible [153–156], the experimental results [178–180] and theoretical predictions [154–156] again favor the additional hydrogen penetration into the subsurface area. In such configuration both surface and subsurface palladium layers participate in the bonding to hydrogen; the hydrogen atoms in both layers are even decoupled due to the increased interlayer distance between the topmost and the second layers. The similar effect of hydrogen dissolution may be induced by co-adsorption of other adsorbates [181].

In particular case of the crystallographically “open” Pd(110) surface the hydrogen penetration into subsurface region and dissolution in the bulk are closely

connected with surface reconstruction. The experimental evidence for the formation of a subsurface hydrogen species on the Pd(110) single crystal surface was obtained at 130 K and high hydrogen loading [115]. The thermodesorption spectroscopy [115,116] reveals a total of four hydrogen binding states. Two high-temperature states (β_1, β_2) are produced by chemisorbed H whereas the low-temperature states (α_1, α_2) only occur on the reconstructed surface and are tentatively attributed to H-atoms that have moved to SS located below the topmost Pd layer. No adsorbed states were obtained below an unreconstructed surface. The DFT calculations [103] showed that, while the MR structure lays slightly lower, the PR and the MR reconstructed surfaces and the unreconstructed phase containing hydrogen atoms in SS have very similar energies. The uncommon PR structure, induced by an incompletely screened Coulomb repulsion between adjacent rows, opens hydrogen diffusion channels into the bulk.

4.4. Electronic structure

Analysis of the electronic structure reveals that the main features are very similar for hydrogen adsorption on all three surfaces. The crystal orbital overlap population curves show that in the Pd(111)–H system the predominant Pd–H bonding character is contained in the split-off band below the Pd 4d band and indicates that the 5sp and 4d orbitals of Pd have rather equal contribution to the Pd–H bond [149,150]. The charge transfer to or from the surface is roughly zero, however, the distribution of electrons near the surface is modified: the d-occupation at the surface is enhanced by 0.09 electron and is compensated by a reduced sp-occupation. The ultraviolet photoelectron spectra from hydrogen adsorbed on Pd(111) indicate the presence of paramagnon satellites [182]. Unfortunately, magnetic properties of the system were not studied by high-level quantum chemical methods.

The site preference for hydrogen adsorption on the Pd(100) is attributed to a maximum gain of covalent bonding energy resulting from the overlap of the hydrogen s- and the metal $d_{x^2-y^2}$ orbitals and from a minimal Pauli repulsion. The interaction between H 1s states and the metal 4d states was mentioned to be strongly dependent on the adsorption geometry [157,158]. The TB calculations [183,184] indicate that

the coupling strength between the 1s orbital of H and the 5s orbital of Pd is an essential parameter as well. For the most stable arrangements the work function increases with coverage up to $\theta = 1.25$ and slightly decreases at higher coverages since hydrogen in subsurface positions tends to decrease the work function [97,154–156]. The alteration of the work function has its origin in the accumulation of screening charge in the surface region.

The arrangement of hydrogen atoms on the unreconstructed Pd(110) surface can be explained by the electronic factors as well. In accordance with the LEED data [119], on the Pd(110) at $\theta=1$ the most stable arrangement corresponds to the zigzag configuration of hydrogen atoms along the Pd[110] rows; the linear superstructure appears to be 0.029 eV/H less stable [160,161]. Detailed analysis of the SCF eigenvalue spectrum obtained within the cluster approximation [146] showed that the H 1s interactions with $4d_{xy}$ and 5s orbitals of the first-row palladium atoms play the most important role in the formation of the surface complexes in the both cases. The stabilizing H–H interaction for the zigzag arrangement may be partially attributed to the reduced Coulomb repulsion due to the large distance between nearest H-atoms, however, the main effect arises from the hydrogen-induced modification of the electronic structure of the topmost-layer palladium atoms, which leads to significantly better overlapping with nearest-neighboring H-atoms in the zigzag configuration than in the linear one (Fig. 4). Such modification leads to the significant decrease of the electronic density localized on each hydrogen atom and its redistribution along the H–Pd–H bonds. Obviously, similar hydrogen-induced changes in the electronic structure of the adsorbent underlie the indirect interactions of surface hydrogen atoms mentioned above.

It was observed that the reactivity of surface hydrogen atoms increases when surface is crystallographically more “open” [138–141]. Two main factors determining the reactivity of an adsorbate are energetics of its adsorption in the most reactive surface sites and its ability to get the reaction center. The mobility of surface hydrogen on different surfaces shows counterintuitive tendency. It appears that the barrier for surface diffusion decreases from 0.19 to 0.12 and to 0.1 eV when moving from (111) to (100) and to (110) palladium crystal planes and the marked

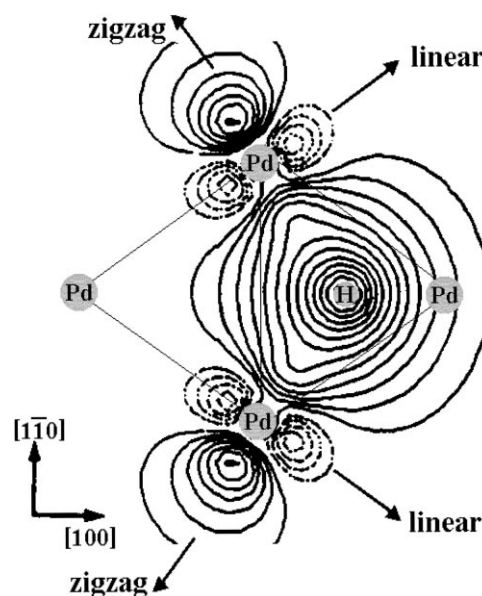


Fig. 4. Wave function contour plot of the split-off level responsible for the Pd–H bonding in Pd_{12}H ; cut parallel to the surface across the first layer palladium atom. Adopted from [146].

surface anisotropy of the (110) surface has no influence on the hydrogen diffusion [159]. The most weakly bound and most reactive form of hydrogen atoms on all surfaces corresponds to its coordination in the top positions. Unfortunately, this surface site attracts only limited attention due to its instability. At the ML coverage the hydrogen adsorption energies in the top positions on the low-index surfaces are very similar [159], however, available computational results allow one to suggest that they are strongly coverage-dependent. Cluster calculations within EHT approximation show [148] that the energetics of the most stable adsorption at the zero-coverage limit is very close to that at higher coverages, in agreement with coverage-dependencies obtained at the DFT level of theory [92,149,151], whereas the stability of the most reactive top sites is significantly higher. At the zero-coverage limit the hydrogen adsorption energy in the top positions decreases from 0.32 to 0.24 and to 0.21 eV when moving from (111) to (100) and to (110) faces. As long as the low hydrogen coverage is better consistent with reaction conditions, destabilization of the hydrogen–palladium interaction together with the easier surface diffusion favors the higher

activity of surface hydrogen on the Pd(110) surface as compared with more close-packed structures.

5. Hydrogen dissociation on palladium surfaces

It is generally accepted that hydrogen dissociation is the first step in the catalytic hydrogenation. The primary step in the process is the collision of hydrogen molecule with surface followed by trapping and sticking. The molecular beam experiments [185] show that the hydrogen sticking probability to palladium surfaces first decreases with increasing kinetic energy of the beam and then increases with the beam energy. Such a behavior is attributed to coexistence of two reaction mechanisms: the direct activated dissociation and the precursor mediated mechanism with molecular pre-adsorption state. The decrease in sticking probability is ascribed to dynamical steering effect, i.e. at low kinetic energies, molecules impinging in an unfavorable configuration are redirected and re-oriented by the corrugation and anisotropy of the PES to non-activated pathways leading to the high sticking probability. At higher energies the sticking probability rises again indicating that the adsorption via direct activated paths becomes dominant.

Within the Born–Oppenheimer and rigid-substrate approximations the PES for dissociative adsorption of hydrogen is a six-dimensional hypersurface. At present its calculation is still a numerically prohibitive task for high-level quantum chemical methods. Thus, at the first stage DFT studies of the reaction paths are concentrated on some low-dimensional cuts, from

which the high-dimensional PES can be built by interpolation. Such studies attract significant attention in the last decade and a number of excellent recent reviews on dynamic effects in dissociative adsorption/associative desorption of H_2 on transition-metal surfaces already exist [187–190]. Therefore, the rotational and translational effects driving a H_2 molecule into favorable pathways in the low beam energy regime will be only briefly compared here; the interested reader is encouraged to refer to the above reviews for more in-depth discussions. First, several reaction pathways with hydrogen molecule oriented parallel to the surfaces and approaching the surface in the perpendicular direction above different well-defined adsorption sites will be analyzed. Along these planes two degree of freedom — the height of the molecule, h , and the H–H distance, d_{H-H} are varied, and lines of constant potential energy are displayed. Two typical PES cross-sections, so-called “elbow” plots, are shown in Fig. 5. Cut-offs of these PES’s along the bottom of the pathway provide energy dependence on the reaction coordinate with the saddle point (if any) corresponding to an activation barrier. According to the Polanyi rules [191], an “early” barrier located in the entrance channel and a “late” barrier located in the exit channel can be distinguished. After that, motion across the surface and angular rotation of H_2 molecule will be considered.

5.1. The 2D PES cross-sections and surface motion

Since calculation of PES and location of the transition state are computationally much more demanding

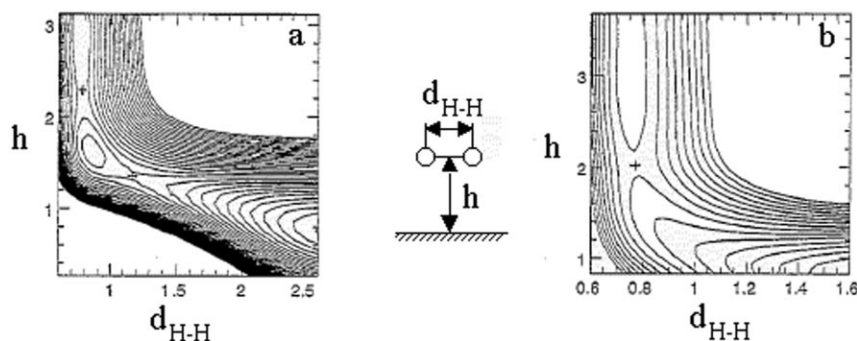


Fig. 5. The 2D potential energy surfaces (PES) for hydrogen dissociation along the fcc–fcc (a) and fcc–hcp (b) reaction pathways. Reproduced with permission from W. Dong, G. Kresse, J. Hafner, J. Mol. Catal. A 119 (1997) 69.

Table 5

Transition and precursor states for hydrogen dissociation on palladium surfaces: activation barriers (E_a^\ddagger , eV), adsorption energies of precursor states (E_{ad} , eV), height of H₂ molecule above the surface (h , Å) and H–H bond length (d_{H-H} , Å)

	Pathway ^a	“Early” TS			Precursor state			“Late” TS		
		E_a^\ddagger ^b	h	d_{H-H}	E_{ad} ^c	h	d_{H-H}	E_a^\ddagger ^d	h	d_{H-H}
Pd(1 1 1) [200,201]	fcc–fcc	0.04	2.30	0.78	0.21	1.75	0.83	0.12	1.38	1.06
	hcp–hcp	0.05	2.27	0.78	0.12	1.59	0.86	0.14	1.37	1.08
	Bridge–top–bridge				0.21	1.80	0.82	0.21	1.45	1.35
	fcc–top–hcp				0.21	1.74	0.84	0.21	1.45	1.35
	Top–top	0.06	2.24	0.79	0.05	~1.84	0.83	0.29	1.58	1.53
	fcc–hcp	0.02	1.93	0.78						
	Bridge–bridge	0.02	1.93	0.79						
Pd(1 0 0) [202]	Hollow–top–hollow				0.12	1.89	0.80	0.37	1.42	1.41
	Bridge–top–bridge				0.27	1.73	0.84	0.37	1.73	0.84
	Top–bond–top	0.01	2.26	0.78	0.21	1.46	0.94			
	Hollow–bond–hollow	0.01	2.16	0.77						
	Bond–hollow–bond	0.09	1.90	0.78						
	Bond–bond	0.00	2.26	0.75						
Pd(1 1 0) [204]	SB–top–SB				0.36	1.80	0.80	0.33	1.42	1.42
	PTF–top–PTF				0.38	1.80	0.80	0.42	1.36	1.60
	LB–top–LB				0.35	1.80	0.80	0.53	0.99	2.49
	PTF–PTF	0.01	1.03	1.32						
	Hollow–LB–hollow	0.08	0.63	0.87						
	PTF–SB–PTF ^e	–0.16	1.14	0.94						
	Top–SB–top	0.21	1.49	1.98						
	LB–hollow–LB	0.31	0.75	0.84						

^aPTF: pseudo-three-fold, SB: short bridge, LB: long bridge positions.

$${}^b E_a^\ddagger = E_{H_2/Pd} - E_{H_2} - E_{Pd}$$

$${}^c E_{ad} = E_{H_2} + E_{Pd} - E_{H_2/Pd}$$

$${}^d E_a^\ddagger = E_{H_2/Pd} - E_{ad}$$

^eNo precursor state was reported by the authors [204] for this reaction pathway, however, small minimum preceding the hydrogen dissociation is clearly visible on the corresponding potential energy profile (see Fig. 3b,c, curve 6 in [204]).

The equilibrium bond length of H₂ is 0.75 Å.

than determination of local minima on the PES, the size of model clusters used for modeling of hydrogen dissociation on palladium surfaces within ab initio cluster approximation [145,192–199] was limited to four atoms. Obviously, such studies might only qualitatively predict the nature of the surface reaction; specific features connected with extremely small size of metal particles are of paramount importance in such small systems. Thus, the present consideration is restricted to the recent periodic DFT calculations performed within GGA approximation for coverages $\theta = 2/3$, $1/2$ – 1 and $1/2$ on the Pd(1 1 1) [200,201], (1 0 0) [202,203] and (1 1 0) [204], respectively. In all these calculations the substrate was kept at the truncated bulk geometry with the calculated equilibrium lattice constant. The energetic and geometric characteristics

of the transition and precursor states obtained in these studies for several reaction pathways are collected in Table 5. Here the same nomenclature as in the original papers [200–202,204] is applied, i.e. the dissociation pathways are specified explicitly by the sites for which head the two H-atoms and for the path names with three items, the middle one specifies the position of the center of mass (see Fig. 1 for notations).

On the Pd(1 1 1) surface, the fcc–fcc, hcp–hcp, bridge–top–bridge, and fcc–top–hcp dissociation pathways constitute of two stages with energies along the reaction coordinate being always lower than that of the isolated H₂ and Pd(1 1 1). The typical “elbow” plot for the fcc–fcc path is shown in Fig. 5a. There are two transition states along these reaction paths. The former transition states located in the entrance

channel are characterized by high adsorption height, negligible elongation of the H–H bond and very low activation energy. These transition states precede the formation of the molecularly adsorbed hydrogen (precursor states), detached from each other by an energy barrier. The adsorption energies of the precursor states are well consistent with the beam energy, at which the minimal sticking probability was observed [185,186]. The latter transition states, located in the exit channel, are connected with the hydrogen dissociation. In these transition states a hydrogen molecule is at a quite short distance to the surface and the H–H bond is significantly stretched. Overcoming these “late” transition state, hydrogen adsorbs atomically on the surface with the geometry and energetics of the end configurations discussed above. The top–top reaction pathway also includes the precursor state with both transition states being higher than those for other two-stage paths, with lower energy gain in the precursor state and with the endothermic end configuration for the atomic adsorption. Finally, along the fcc–hcp and bridge–bridge pathways the reaction proceeds without a precursor state (see Fig. 5b for an example of 2D cuts for such pathways). There are small activation barriers in the entrance channel, which agree fairly well with the estimation based on the molecular beam experiments, 50 meV.

Several coordination sites with low or no barriers to hydrogen dissociation were located on the Pd(100) surface [202,203]. The dissociation over the bridge–bridge pathway proceeds with a continuous gain of energy without a hampering energy barrier. Another two energetically favorable reaction paths, hollow–bridge–hollow and top–bridge–top, with very small activation barrier correspond to the hydrogen molecule dissociating at the bridge position with the H₂ molecular axis being perpendicular and parallel to the Pd–Pd bond, respectively. The bridge–hollow–bridge reaction pathway also has small activation barrier. All these transition states are located in the entrance channel with higher barrier being located closer to the surface and accompanied by stronger perturbation in the adsorbed molecule. The dissociation of a hydrogen molecule over the top site with hollow–top–hollow and bridge–top–bridge orientation is precursor mediated; in the precursor state the adsorbed molecule is more activated in the deeper well. The precursor well with the bridge–top–bridge

orientation is the most attractive site far from the surface, i.e. molecules are first steered towards there. However, hydrogen dissociation in the top site is significantly activated. The most favorable reaction pathways for further hydrogen interaction with the surface was found when the molecule was allowed to change its position above the surface in the parallel plane, i.e. then high-dimensional (at least 3D) PESs were analyzed. Motion across the surface and rotation are able to take the molecule to a lower potential. The preferential reaction channel for hydrogen dissociation on the Pd(100) plane includes the capture of H₂ molecule in the molecular adsorption state with the bridge–top–bridge orientation followed by steering into the bridge–bridge geometry, dissociation and surface diffusion of the separated atoms towards the final hollow positions [202].

Similarly, on the Pd(110) surface almost non-activated, activated and precursor mediated reaction pathways were found for a hydrogen molecule dissociation [204]. The most favorable reaction pathway corresponds to pseudo-three-fold-short bridge-pseudo-three-fold orientation of the H₂ molecule above the surface with the molecular axis being perpendicular to the [1 $\bar{1}$ 0] rows. The precursor state, which presents a molecular adsorbed state of hydrogen on the Pd(110) surface, appears to be significantly more stable than the precursor states on the Pd(111) and Pd(100). Such relationship was expected based on the molecular beam experiments [185]. This precursor state is formed without an activation barrier along different reaction pathways with the H₂ center of mass located above a Pd atom. In the precursor well the hydrogen molecule can rotate almost freely in the plane parallel to the surface with very small rotational barrier of 0.03 eV, however, for all orientations the direct hydrogen dissociation from the precursor state is hindered by a high activation barrier. The lowest energy pathway linking this precursor state to the final adsorbed state requires a considerable steering of the molecule, which consists of sliding parallel to the surface in the [1 $\bar{1}$ 0] direction with hydrogen molecule oriented perpendicular to the Pd[1 $\bar{1}$ 0] rows. This way the center of the molecule reaches the short bridge position located 0.20 eV above the precursor state, which presents the transition state for such precursor mediated reaction pathway. The end configuration with two hydrogen

atoms in pseudo-three-fold positions sharing the short bridge Pd–Pd bond is by 0.106 eV higher in energy than the most stable structure with zigzag arrangement of hydrogen atoms along the Pd[1 $\bar{1}$ 0] rows. This ground state structure is available via easy-going surface diffusion of the adsorbed hydrogen atoms.

Comparing the mechanisms and energetics of hydrogen adsorption on low-index palladium surfaces one can see that geometric factor plays an important role in hydrogen dissociation. While the most attractive states for hydrogen capping far from the surfaces are relatively weakly bound precursor states, the most important difference we would like to stress here is increasing stability of the molecular adsorption state on more crystallographically “open” faces. This state is further stabilized by the increasing energetic barrier to hydrogen dissociation from the precursor state along the reaction pathways perpendicular to the surface. Geometric parameters of the surfaces and of the particular adsorption sites determine overlapping between bonding and antibonding orbitals of H₂ and those of the substrate and thus, control the geometry and energetics of the precursor and transition states. Along the reaction coordinate the energetic levels of σ - and σ^* -MO of hydrogen drop quickly due to the interaction with the surface atoms. The higher the energetic benefit provided by the interaction of the σ -bonding orbital of H₂ with orbitals of palladium the closer to the surface the adsorbed molecule can approach without a hampering energy barrier. This situation corresponds to the “early” transition state. For the top-centered coordination sites the σ -MO of hydrogen interacts mainly with the 4d_{z²}-AO of palladium. This orbital becomes available for interaction with incoming hydrogen molecule at longer distance from the surface than other 4d orbitals, but it provides relatively small stabilization of the σ -bonding orbital of H₂ in the transition state that underlies the formation of the precursor state and relatively high activation barrier for hydrogen dissociation. Thus, at the transition states, the energetic ordering of the dissociation pathways can be accounted for by the strength of orbital interaction between the σ -bonding orbital of H₂ and those of the substrate. The σ^* -MO is empty in the free molecule; at the transition state this MO reaches the Fermi level of the surface and becomes occupied. The stretching of H₂ molecule is determined by filling of its σ^* -MO.

Larger stretching of the hydrogen molecule bond leads to a higher barrier for hydrogen dissociation.

5.2. Out-of-plane rotation

The six-dimensional dynamic calculations of hydrogen adsorption on the Pd(1 1 1) [187] and (1 0 0) [205–207] surfaces, as well as the beam experiments [208], show that a rotation of the hydrogen molecule moving its molecular axis out of the plane parallel to the surface gives rise to a sharp increase of energy. However, the dynamics of hydrogen interactions with palladium surfaces are complicated by the presence of the subsurface channel. The experiments [209] tell us that hydrogen molecule can dissociate and absorb directly into the palladium bulk, without equilibrating in the chemisorption well. Though this reaction channel does not lead straightly to the most stable end configuration, the direct subsurface absorption of hydrogen on the Pd(1 1 1) surface was extensively studied [210–213]. The analysis of the 3D PES including an angular degree of freedom for a H₂ molecule interacting with the Pd(1 1 1) surface showed that there is an entrance channel barrier of about 0.09 eV to both dissociative chemisorption and direct subsurface absorption, but after this barrier is crossed direct subsurface absorption proceeds with an activation barrier as small as 0.02 eV. In the low-energy regime rotation inhibits direct subsurface absorption at low rotational states and promotes it at high rotational states [213], however, a large part of the hydrogen goes directly subsurface even at low incident kinetic energies. As it was shown for the Pd(1 1 1) [214] and (1 0 0) [202] surfaces, this reaction channel enables the occupation of mixed surface and subsurface states.

5.3. Poisoning of palladium catalysts in reactions of hydrogenation

Poisoning of catalysts is an extremely important issue for their practical applications. The most accepted explanation of this phenomenon originated from extensive experimental investigations is blocking of available or most active catalytic sites on a surface. Theoretical results allow deeper insight on the phenomenon. In this section we will compare the geometric and electronic factors of poisoning the hydrogen activation on sulfur, chlorine and potassium doped palladium surfaces.

Experimentally, it is well known that the presence of sulfur on palladium surfaces leads to a large reduction of catalytic activity in hydrogenation reactions in general and of the hydrogen dissociation probability in particular [185,186,215]. Chlorine compounds, contrary, are known to impart some degree of thio-resistance to hydrogenation catalysts [216]. The theoretical study of the aspects of poisoning and promotion on the Pd(1 1 1) surface was performed by periodic calculations within GGA approximation [93,217,218]. On the Pd(1 1 1) surface both sulfur and chlorine occupy highly coordinated sites with the latter being significantly weaker bound. In accordance with the scanning tunneling spectroscopy data, sulfur atoms adsorbed in fcc and hcp sites show small energetic and geometric differences [219]. The interaction between sulfur and palladium leads to the outward relaxation on the surface while chlorine adsorption causes its inward relaxation. The sulfur–palladium bonding is essentially covalent; the chlorine–palladium interaction is more ionic in character. At coverage $\theta = 0.11$ both sulfur and chlorine induce increase in the work function of 0.13 and 0.23 eV, respectively, and of 0.27 eV for co-adsorption. Though the interaction between sulfur adatom and the surface are localized to palladium atoms bound to the adatom, the electronic character of surface atoms not directly linked to the S-atoms is also changed, showing increased occupation of the s-hybridized electronic states perpendicular to the surface. These states are unoccupied on the clean palladium and thus, an incident molecule will experience increasing Pauli repulsion on the sulfur-poisoned surface. Chlorine adsorption causes less pronounced alterations. As a result of such changes, both sulfur and chlorine destabilize the molecular adsorption state of hydrogen and give rise to the activation energy for the hydrogen dissociation.

On the poisoned surface, the hydrogen adsorption in any site that involves palladium atoms directly bound to sulfur becomes disabled. Thus, at low coverages each sulfur atom strongly perturbs up to 13 three-fold sites. For some of these sites dissociative adsorption of hydrogen becomes endothermic and for others the binding energy is significantly reduced. The barrier for hydrogen surface diffusion strongly increases in the near-sulfur region. For sulfur coverage of 0.33 ML the hydrogen binding energy is reduced by more than 0.5 eV. That makes hydrogen adsorption unstable

with respect to associative desorption and the surface is completely poisoned, in agreement with the experimental observations. Promoting effect of chlorine at high coverages on the Pd(1 1 1) surface is assigned to the reduced Cl–Cl repulsion compared with S–S and S–Cl interactions. At the same chlorine coverage the decrease in the hydrogen binding energy is only 0.3 eV and the hydrogen dissociative adsorption is still energetically favorable. The ethylene adsorption on Pd(1 1 1) surface was found to be slightly weakened by sulfur but not by chlorine; co-adsorption of Cl atoms on S-covered surface increases the ethylene binding energy [217]. These results together with experimental observation on strong poisoning of Pd-based catalysts firmly support the hypothesis that poisoning of hydrogenation catalysts influence mainly the stage of hydrogen activation.

The poisoning of hydrogen dissociation on the Pd(100) by sulfur adsorption has been the subject of detailed DFT [220–223] and ab initio quantum and molecular dynamic simulations [224,225]. As in the case of Pd(1 1 1) surface, S-atoms occupy the highly coordinated hollow sites and induce an activation barrier to hydrogen dissociation. For coverage $\theta_S = 0.25$ the minimum barrier of 0.1 eV corresponds to H₂ approach towards the four-fold hollow site, which is farthest away from the sulfur atoms. For the bridge approach geometry (almost non-activated on the clean Pd(100)) a barrier of 0.15 eV hinders the dissociation at the sulfur-covered surface. The hydrogen binding energy becomes lower in the presence of sulfur, however, the hydrogen dissociation is still exothermic. These results indicate that poisoning of the Pd(100) surface is not due to a site blocking but may be explained by combination of two effects: indirect sulfur-induced downshift of the Pd d-bands resulting in a larger occupation of hydrogen-surface antibonding states and direct repulsive interaction of hydrogen molecule with sulfur atom. For $\theta_S = 0.5$ the PES for hydrogen dissociation becomes purely repulsive since in all possible adsorption geometries the hydrogen molecules come too close to the sulfur adatoms before the dissociation is completed.

Potassium atoms adsorbed on the Pd(100) surface occupy surface hollow sites and cause strong decrease of the metal work function (about 4 eV for $\theta = 1/4$ ML) [226]. At this coverage potassium induces the energy barrier for dissociation of 0.18 eV in the entrance

channel of the PES. When the H_2 molecule is dissociated, potassium tends to stabilize the H-substrate bond. For the most stable on clean Pd(100) surface hollow position this stabilization is very small, but two-fold bridge position becomes 0.16 eV more stable. That lead to the change of the preferential position for hydrogen adsorption on potassium-covered Pd(100) surface and to significant increase in its adsorption energy. Both inhibiting and stabilizing effects are in agreement with the experimental observations [227].

The general conclusion from the above results is that the main reason of poisoning by sulfur and potassium is associated with dopant-induced occupation of Pd 5s orbitals, which prevent primarily the capping of incoming hydrogen molecule. In addition to the precursor state, sulfur destabilizes an atomic hydrogen adsorption. On the close-packed (111) surface site blocking is more pronounced than on the more “open” (100) due to a shorter distance between nearest adsorption sites and thus, their stronger interaction.

6. Palladium cluster catalysts

The high ratio of surface area to volume makes ultradispersed transition-metal particles (clusters) extremely attractive for catalytic applications. Clusters presents an intermediate state between molecules and solids and their catalytic properties combine advantages of homogeneous and heterogeneous catalysts. Since the surface structure of clusters is usually more uniform than that of bulk metals, their selectivity is close to that in homogeneous reactions. On the other hand, in immobilization on solid supports, they are as easy to handle as heterogeneous catalysts. Moreover, due to the specific geometric and electronic structures, clusters show several unique catalytic properties determined exclusively by their extra-small size. Palladium clusters are among the most promising nano-sized catalysts in various applications. Ultradispersed palladium clusters supported on alumina, for example, were found to be more active than Pd(111) single crystals in CO oxidation by oxygen [228]. The catalytic reduction of nitrogen monoxide with propane on zeolite-supported palladium clusters [229,230], as well as the extremely active NO reduction by CO on highly-dispersed palladium clusters supported on γ -alumina [231], are the key reactions in the exhaust

gas treatment. Furthermore, ultradispersed supported palladium clusters of up to 2 nm (150 atoms) in size, are the active catalysts in hydrogenation processes [232] having a much higher selectivity with respect to the conversion of triple to double bond than that of bulk palladium [233]. In contrast to the bulk metal, small palladium clusters with diameter $d \leq 25 \text{ \AA}$ show no ability to hydrogen dissolution [234–236]. Except of supported cluster catalysts, very interesting from the fundamental point of view catalytic nano-cluster systems, working while dispersed in solution, present giant cationic palladium clusters with the approximate formulas $Pd_{561}L_{60}(OAc)_{180}$ ($L = 1,10$ -phenanthroline (phen) or 2,2'-bipyridine) and $Pd_{561}phen_{60}O_{60}(PF_6)_{60}$ [237–241]. These clusters have been extensively characterized and tested in a number of catalytic reactions.

Several comprehensive reviews on transition-metal nano-particles and their applications in catalysis were published recently [241–243]. Therefore, in this section we will consider only the most salient features of the geometric and electronic structures of small palladium clusters, which allow one to better understand the size-dependencies of their chemisorptive and catalytic properties and to separate the structure-dependent effects of highly-dispersed catalysts (intermetallic bond length, bulk and surface structures) from size-dependent ones (large surface area, strong influence of support). This information may be used in future investigations on the influence of certain supports and adsorbates on the structure of highly-dispersed palladium clusters in specific catalytic reactions. Different theoretical approaches and experimental techniques have been used to study the electronic structure and geometries of ultradispersed palladium clusters. Extremely small size of cluster catalysts makes experimental methods based on diffraction techniques not useful to elucidate their structure. Contrary, theoretical studies become highly efficient because small size of cluster particles enables their direct calculations and a complete minimization of the total energy with respect to all the atomic positions. In contrast to the single crystal bulk surfaces, the structure of nano-sized cluster particles is not uniquely determined. Therefore, the available data on bulk and surface geometries of small palladium clusters will be considered first in this section. Then we will switch to the closely related question of their specific electronic

properties. Finally, we will follow the influence of geometric and electronic structure of small palladium clusters on their interaction with hydrogen.

6.1. Bulk and surface geometry of small palladium clusters

Small transition-metal particles often exhibit unusual symmetries and contracted lattice parameters as compared with those of bulk metal [232]. Among all uncommon arrangements there is a strong tendency to develop pentagonal symmetry. The microstructure of nano-crystalline palladium shows high density of twins, small angle boundaries, dislocations and bent regions [244]. The twins formation was found for highly-dispersed palladium deposits on different supports [244–248], in nano-crystalline palladium prepared in the gas-phase [249], in thin Pd films deposited on mica [250] and in Pd alloys [251,252]. The Pd/NaY catalysts were shown to contain mainly small palladium clusters identified as Pd₁₃ icosahedron [253]. In the case of Pd grown epitaxially on a metal oxide surface at low-temperatures, on the other hand, the 2D islands growth is often followed by 3D clustering from a critical submonolayer coverage [248]. Structural transformations in Pd clusters are accompanied by changes in their catalytic activity.

The electronic structure, geometries and energies of Pd clusters have been widely studied by molecular dynamic simulations [254–258]. The influence of cluster symmetry was addressed by comparing the cubo-octahedral structure (fcc type) with the icosahedral one (five-fold symmetry), which is adopted by small clusters. Pd cubo-octahedral and icosahedral clusters were shown to undergo an inhomogeneous contraction, restricted to the surface edge and, in the latter case, to the inner core [257]. In the framework of corrected effective medium methods, the dominance of the five-fold symmetry clusters with contracted interatomic distances, was found for the Pd_n clusters with *n* from 7 to 19 [259].

In the recent spd TB model calculations of large palladium clusters containing up to 201 atoms [109] a contraction of the equilibrium bond length with respect to the bulk one was obtained. This contraction decreases with increase of cluster-size and the authors explain this trend by the increase of average coordination. The icosahedron was found to be more stable

than the cubo-octahedron and the binding energy per atom increased with the average coordination. A massively parallel ab initio computer code, which uses Gaussian bases, pseudo-potentials, and the LDA, was employed for the study of Pd_n (*n* = 55, 135, and 140) clusters with icosahedral and fcc structures [260]. Remarkably large compressions of the central atoms were observed for the icosahedral structures (up to 6% compared with bulk interatomic spacing), while small-core compressions (~1%) were found for the fcc geometry. In contrast, large surface compressive relaxation was found for the fcc clusters (~2–3% in average nearest neighbor spacing), while the icosahedral surface displays small compressions (~1%). For *n* = 55 and 135 the icosahedral structures were preferred, while for *n* = 140 the octahedron was found to be slightly more stable.

High-level quantum chemical investigations of ultradispersed transition-metal particles are the way of choice for such studies, but they are still computationally very expensive and, therefore, are applied for very small clusters. Another difficulty of dealing with transition-metal clusters arises from the fact that a variety of geometries and electronic states can have very close energy for a given cluster-size. This requires the computationally very expensive frequency calculations to be performed for each geometry. To the best of our knowledge, in the particular case of palladium such calculations were reported only for palladium dimer [261], trimer [262] and tetramer [263,265]. The geometries of two–five atomic clusters were optimized at post-Hartree–Fock level [287–291], however, the symmetry constraints applied in these studies for Pd₄ and Pd₅ clusters do not correspond to the lowest energy configurations. Lately, full geometry optimization of up to six atomic palladium clusters have been performed using DFT method while allowing for the occurrence of low-symmetry structures [266]. The formation of close-packing 3D configurations with metal–metal bond lengths slightly smaller than those of the bulk palladium were confirmed in these calculations. DFT results concerning the geometry of Pd₁₃ clusters [267,268] are conflicting and not comparable with the results for smaller clusters. Therefore, available high-level theoretical results do not answer whether small palladium clusters growth in either the cubo-octahedral or icosahedral configurations and which factors control the equilibrium geometry.

Here we will follow the size-dependent changes in the geometric and electronic structures of the Pd_n ($n = 2\text{--}13$) clusters and their singly positively and negatively charged ions qualitatively, based on the results of the EH calculations with an electrostatic two-body correction [269,270]. These calculations indicate that as the size of small neutral Pd_n clusters increases the right triangle ($n = 3$), triangular ($n = 4$) and square ($n = 5$) pyramids (or triangular bipyramid with very close energy), octahedron ($n = 6$), pentahedral bipyramid ($n = 7$), and slightly distorted icosahedron ($n = 13$) are formed consecutively. The surfaces of these clusters have primarily triangular structure like a curved (1 1 1) crystal face; the more crystallographically “open” square planar surfaces are absent (except of square-pyramid Pd_5 structure). These geometries are well consistent with the high-level results for very small clusters with $n \leq 6$ mentioned above and are further confirmed by DFT calculations for larger clusters [271]. In all calculations the contraction of interatomic distances as compared with the bulk palladium was obtained, but no clearly defined size-dependence of the Pd–Pd bond length was observed. The stability of small palladium clusters tends to increase with size.

Such geometric structures correspond to the minimal energy configurations of palladium atoms, however, very close energies of different structures makes their interconversion easy, especially in the case of a few atomic clusters. Thus, an interaction with support and adsorbates can lead to strong changes in the cluster shape and electronic configuration due to the pronounced charging and formation of new chemical bonds. Indeed, charging of highly-dispersed palladium particles was found to cause the strongest changes of their geometric and electronic structure. Fig. 6 shows the minimal energy configuration of Pd_n^+ , Pd_n^0 and Pd_n^- (n varies from 2 to 13) clusters, their optimized shortest bond lengths, binding energies per atom and ionization potentials approximated as a level of the highest occupied molecular orbital (HOMO). The symmetry of the ground state configurations of neutral and anionic clusters are, in general, equivalent. The cationic clusters with six or less atoms, on the other hand, tend to form planar structures. As the cluster grows the energetic difference between these minimal energy structures and the 3D ones becomes smaller and cationic Pd_n^+ clusters with $n \geq 7$ prefer the same symmetry configurations as the neutral and

negatively charged ones. Such reconstruction of Pd_n^+ cations may be explained by a relative decrease in the electron deficiency with increase of the cluster-size. However, excess and deficit of electron density influence the relative stability of different configurations even in the bigger clusters. For instance, for anionic 7, 9, and 13 atomic palladium clusters the pentagonal symmetry configurations and twins are 0.225, 0.191 and 0.089 eV more stable than the clusters with bulk fcc lattice. For cationic clusters the differences are 0.007, 0.056 and 0.075 eV, much smaller than those for the corresponding anions and changing in the opposite direction. Both positive and negative charges lead to the strengthening of Pd–Pd bonds, but their influence decreases as the cluster grows. Due to the interplay of these two effects, the singly charged cationic and anionic Pd_3 clusters show the strongest intermetallic binding. The intermetallic distances in both positively and negatively charged clusters are significantly shorter than those in the corresponding neutral clusters, while the binding energy per atom in the charged clusters is much higher. The smaller the cluster-size the more pronounced are these changes.

Comparing with other transition-metal clusters, very close similarity in the geometric and electronic features of the Pd_n and Rh_n ($n \leq 13$) [272] clusters have to be noted. For the platinum clusters with two–six atoms [273], on the other hand, the formation of planar structures was found to be preferential. Their further growth leads to a variety of disordered configurations with very similar energies as a minimum energy isomers of Pt_{13} , which, however, were not observed experimentally. The Ni_n clusters with n from 2 to 7 [274,275] present an intermediate situation, i.e. square planar and 3D (D_{2d} symmetry) configurations of Ni_4 and pentagonal bipyramid and octahedron with an atom capping one of the faces for Ni_7 are nearly degenerated, while other nickel clusters have the similar shape as rhodium and palladium ones.

6.2. Electronic structure of small palladium clusters

The main characteristic features of the electronic structure of atomic scale palladium particles are significant split in the valence d-zone and the energetic gap between occupied and vacant zones. As the cluster grows, its HOMO, which presents the top of the filled d-zone, tends to rise. The lowest unoccupied molecular

n	parameter	Pd_n^+	Pd_n^0	Pd_n^-
2	r_e	2.221	2.489	2.191
	BE/at	0.307	0.068	0.685
	IP	-11.43	-11.62	-8.67
3	r_e	2.318	2.529	2.346
	BE/at	0.350	0.113	0.720
	IP	-11.16	-11.45	-9.26
4	r_e	2.316	2.570	2.427
	BE/at	0.336	0.144	0.711
	IP	-11.14	-11.50	-9.68
5	r_e	2.355	2.519	2.434
	BE/at	0.323	0.167	0.666
	IP	-10.98	-11.40	-9.89
6	r_e	2.372	2.595	2.496
	BE/at	0.308	0.182	0.635
	IP	-10.95	-11.46	-10.11
7	r_e	2.386	2.562	2.478
	BE/at	0.293	0.195	0.596
	IP	-11.22	-11.44	-10.19
13	r_e	2.325	2.564	2.529
	BE/at	0.302	0.230	0.482
	IP	-10.94	-11.24	-10.63

Fig. 6. Minimal energy configuration of Pd_n^+ , Pd_n^0 and Pd_n^- ($n = 2-13$) clusters, their optimized shortest bond lengths, binding energies per atom and ionization potentials (approximated as HOMO level). Reproduced with permission from I. Efremenko, M. Sheintuch, J. Mol. Catal. A 160 (2000) 445.

orbitals (LUMO), which defines the bottom of the s-zone, drops sharply with increasing cluster-size. These two effects cause the narrowing of the forbidden zone and the magnification of metal properties; the energetic gap between 5s- and 4d-zones narrows from 2.732 to 0.548, from 3.217 to 0.68 and from 2.787 to 0.318 eV for anionic, neutral and cationic clusters, respectively, with increasing number of atoms from 2 to 13 [270]. The Mössbauer and NMR spectroscopic investigations as well as conductivity measurements

prove that even 1–3 nm clusters still possess freely mobile electrons, while impedance and scanning tunneling spectroscopy identify 1.4 nm two-shell clusters as species with beginning semiconducting properties [276]. The energy of the lowest valence orbital (LVMO), which represents the bottom of d-zone, decreases slowly with increase of cluster-size inducing the d-zone breadth. In the case of icosahedral cluster growth, d-zone splits into a few narrow bands separated by forbidden zones of up to 0.3 eV wide. In the

cubo-octahedral Pd₁₃ structure the distribution of d orbital levels across the width of the d-zone is more uniform, and the biggest gap is only 0.17 eV wide. As a result of stronger intermetallic interactions in charged clusters, both excess and deficit of the electron density lead to the broadness of the d-zone and, as a sequence, to even more pronounced split in the valence d-zone.

The electron density in small palladium clusters is distributed quite homogeneously and the total charge on atoms does not exceed 0.005. The only exception is the central atom in the icosahedral Pd₁₃ cluster keeping net charge of -0.01 ; the surface atoms in this cluster have very small charges not bigger than ± 0.001 . The bonding character of the highest occupied and antibonding nature of the lowest empty MO underlie the strengthening of small palladium clusters with charging. Occupation of the spherically symmetric diffusive Pd 5s AOs is responsible for the formation of 3D structures, whereas stability of the planar configurations is due to the appearance of vacancy in the valence 4d-shell that promote interactions between spatially localized orbitals. Thus, external interactions with supports, ligands and adsorbates might determine the general direction for the growth of small Pd clusters and make the obtained structures more stable as compared to the corresponding gas-phase clusters. The electron-donors should promote the formation of 3D small palladium particles with the pentagonal symmetry while the electron-seeking surrounding is expected to assist the formation of planar and 3D bulk-like configurations.

Let us illustrate these conclusions by two examples, i.e. the theoretical results on palladium interactions with the Ni(1 1 1) surface and the experimental data on the structure of giant ligand stabilized palladium clusters. Using ASED MO method, the optimal geometrical situation for palladium deposits on Ni(1 1 1) was found to be compact 2D aggregates in pseudo-epitaxy or pseudo-morphy with the underlying Ni surface, depending on the aggregate size. Small 2D aggregates with significantly shortened Pd–Pd bonds are the most stable in the case of a palladium inclusion in the first nickel layer. In both cases a partial filling of the Pd 5s orbital and depletion of the valence d-zone occur, however, deposited palladium atoms are weakly negatively charged while the total charge transfer from palladium to surrounding nickel was obtained in the

case of inclusion [277]. In both cases the optimal geometric structures are determined mainly by overlapping of Pd 4d electrons and by a rather strong interaction between metals. The average charge of Pd atoms in the giant cationic palladium clusters is suggested by authors to be about $+0.3$, in accordance with the idealized formula Pd₅₆₁phen₆₀(OAc)₁₈₀ [241], while TEM, SAXS, electron diffraction and EXAFS studies show the presence of 26 ± 3.5 Å spherical particles with an icosahedral packing order of the metal atoms in the core of cluster. The total number of palladium atoms per clusters estimated experimentally (~ 570) is as well in close agreement with an idealized five-shell icosahedrally packed full-shell cluster ($1 + 12 + 42 + 92 + 162 + 252 = 561$). Such apparent disagreement between the notable positive charging of the cluster and its icosahedral packing can be explained if one will analyze the structure of the cluster shown in Fig. 7a. The metal core in the cluster is surrounded by strong electron-donor phenanthroline ligands. The model DFT calculations at the B3LYP level show that palladium atoms keep significant excess of electron density in such surrounding while the positive charge is localized on the C-atoms of the ligand (Fig. 7b). The similar charge flow remains in the positively charged fragments of the giant cationic palladium clusters shown in Fig. 7c. In the Pd(phen) fragment the only palladium atom has the deficit of electron density of only 0.41 and the total positive charge on metal atoms in the Pd₃(phen)⁺ fragment is significantly lower than it was expected by the experimentalists and is close to that in the cationic Pd₇⁺ cluster presented in Fig. 6.

In many cases nanometer-size transition-metal clusters have demonstrated remarkable magnetic properties that differ from the properties of the individual atoms and of bulk crystalline solids [278–280]. Spin state is a very important factor for many applications, particularly, for catalysis, since all chemical reactions are spin-selective and spin state cannot be changed by chemical interaction. In the specific case of palladium, it may be the key factor, which distinguishes the electronic structure and, as a sequence, the catalytic behavior of cluster catalysts from metallo-complex and bulk ones. Magnetic properties of small palladium clusters were extensively studied. Using a simple TB model with electron–electron interactions, it was found that cubo-octahedral (fcc) and icosahedral Pd₁₃ clusters are non-magnetic in the ground

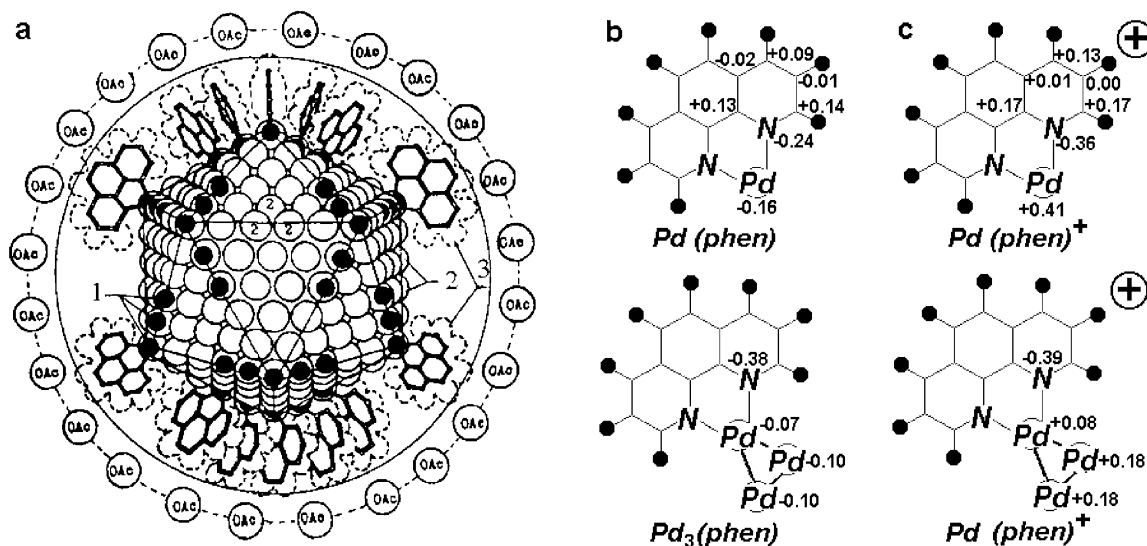


Fig. 7. The idealized model of $\text{Pd}_{561}\text{phen}_{60}(\text{OAc})_{180}$ cluster. Reproduced with permission from M.N. Vargaftik, V.P. Zargorodnikov, I.P. Stolarov, I.I. Moiseev, D.I. Kochubey, V.A. Likholobov, A.L. Chuvilin, K.I. Zamaraev, *J. Mol. Catal.* 53 (1989) 315. (1) Pd atoms coordinated with phenanthroline ligands; (2) Pd atoms accessible for coordination with $(\text{OAc})^-$ anions or molecules of substrates or solvent; (3) van der Waals surface of coordinated phenanthroline ligands (a); Mulliken charges on the neutral (b) and cationic (c) surface fragments of the cluster calculated at the B3LYP level of theory.

state and that the interatomic distances increase by up to approximately 7% between non-magnetic and magnetic species [281,282]. The cubo-octahedral Pd_{13} cluster appears to be more stable and to have small spin polarization by the self-consistent spin-polarized density-functional scheme using the norm-conserving pseudo-potential in the LCAO method [283]. From the Gaussian orbital basis and the local spin-density approximation Pd_{13} (fcc) [284], Pd_{15} (bcc) and Pd_{19} (fcc) [285] clusters are very likely to be magnetic although, the magnetic moment is very small. Both Pd_{43} and Pd_{55} clusters are shown to have magnetic ground states using the discrete-variational local-spin-density-functional method [286].

More rigorous ab initio calculations were performed for smaller systems [287–293]. Balasubramanian and co-workers [287–291] have widely investigated palladium clusters for sizes up to five atoms using multiconfiguration self-consistent field (MCSCF) followed by multireference singles plus doubles configuration interaction (MRSDCI). Spin-orbit effects were included using a relativistic CI method. These calculations show the single palladium atom to have closed-shell separated by 0.6 eV from the lowest triplet state [287]. The

ground state of Pd_2 was found to be $^3\Sigma_u^+$ with Pd–Pd bond length of 2.48 Å and with singlet excitation energy of 0.55 eV [288]. For Pd_3 the lowest energy corresponded to isosceles triangle with the base of 2.47 Å and sides of 2.67 Å in 1A_2 electronic state; these state is by 0.28 and 1.04 eV lower than the most stable triplet and quintet configurations, respectively [289]. The 3D Pd_4 clusters ($d_{\text{Pd-Pd}} \sim 2.69$ Å) with nearly degenerated 3T_1 and 1A_1 states were found to be significantly more stable than planar ones [290], but only tetrahedral symmetry was considered in this work. The edge-capped tetrahedron structure with C_{2v} symmetry in 3B_2 electronic state and the tetragonal pyramid with $d_{\text{Pd-Pd}}$ of 2.61 Å in base and of 2.98 Å in side had about the same energy for considered Pd_5 isomers [291]; planar structures had again much high energy.

Extensive investigation of small palladium clusters was performed with density functional approximation [261,262,266,46,294,295]. In these studies larger clusters were calculated and more reliable geometries with low-symmetry were considered. DFT methods using several gradient-corrected functionals as well as the hybrid B3LYP functional were shown to perform very well for energetic studies of small

palladium clusters [266,294] and their singlet–triplet separation energy [46]. All DFT results indicate that the ground state of Pd atom is a singlet. In spite of some deviations obtained in different approaches and basis sets [46], it is generally accepted now that the palladium dimer has lowest energy in the triplet state [296,294,295]. The ground state of Pd₃ is claimed to be singlet in [46] while in [262,266,294] the triplet ³B₂ state was found to be more stable. The optimized geometries for Pd₂ and Pd₃ clusters are very close to those obtained by Balasubramanian and co-workers. The ground states of Pd₄ and Pd₆ clusters were found to be ³B₂ (in C_{2v} symmetry) and ³B_{2g} (in D_{4h} symmetry), respectively [266]. Trigonal bipyramid and pyramid configurations of Pd₅ cluster in the triplet state appear to be the stable states with energy difference within 1 kcal/mol in DFT calculations using the Vosko–Wilk–Nusair (VWN) exchange–correlation potential with Becke and Perdew non-local gradient corrections [295]. The self-consistent spin-polarized density-functional calculations of Pd₁₃ clusters [267] showed the cubo-octahedral configuration with small Jahn–Teller distortion to be more stable than the icosahedral one. Contrary, the triplet icosahedral cluster distorted by the Jahn–Teller effect was the most stable in the framework of INDO scheme [297]. Using density-functional scheme with the discrete variational method the spin-polarized icosahedral cluster appears to be 0.5 eV more stable than the cubo-octahedral one [268]. Our B3LYP calculations of the Pd_n clusters with $n \leq 13$ [271] confirmed that the closed-shell state is the most stable one only for a single palladium atom, whereas for larger systems higher multiplet states are more stable. The singlet–triplet separation energy oscillates in the range of 0.13–0.74 eV with increase of cluster-size while the energy of the quintet state decreases quickly, so that for the Pd₇ cluster this state becomes more stable than the singlet one. The lowest-energy state of the Pd₁₃ cluster corresponds to the icosahedral configuration, however, the energy difference between cubo-octahedral and icosahedral isomers is very small. Finally, for the model Pd₁₉ cluster used in [295] to represent the Pd(1 1 1) surface the quintet state becomes 0.36 eV more stable than triplet. Thus, although, there is some disagreement concerning the most stable geometry of relatively large palladium clusters, both *ab initio* and DFT results coincide that small palladium clusters have

open-shell electronic configuration, in contrast to the single atom and to the bulk form. Moreover, a high multiplet state of relatively large palladium clusters probably remains at their immobilization on supports [298,299]. The triplet state remains to be more stable than singlet when O-atom is adsorbed on Pd_n with $n \leq 19$ and when ethylene is π -bound to Pd₁₉ [295].

These theoretical predictions promoted the experimental measurements. In several studies [300,301] magnetism of small palladium clusters was not confirmed but, according to Cox et. al. [300], the experiments might not have a sufficient sensitivity. The 4d ferromagnetic ordering in pure Pd nano-particles was observed in the dc magnetic measurements [302]. The magnetization increased rapidly with decreasing particle size and a sample with 59 Å median radius showed a factor of nineteen larger magnetization than that of Pd bulk at 1.8 K. The authors supposed that only the surface monolayers of Pd particles are magnetic and estimated, based on this assumption, the ferromagnetic moment of $0.23 \pm 0.19 \mu\text{B}$ per atom, which is comparable to the value predicted by DFT calculations. In the bulk form palladium is a Stoner-enhanced Pauli paramagnet. The susceptibility of small (10–150 Å) Pd particles was found to decrease strongly with decreasing size [303]. This is in line with the calculated decrease of the triplet–quintet separation energy with increasing cluster-size [271]. The giant cationic ligand stabilized Pd clusters Pd₅₆₁phen₆₀(OAc)₁₈₀ and Pd₅₆₁phen₆₀O₆₀(PF₆)₆₀ [237–240] exhibited a weak, only slightly temperature-dependent paramagnetism within the temperature interval from 77 to 300 K. However, at the temperature $T < 2$ K the electronic magnetic susceptibility was shown to be very high and to decrease rapidly with increasing cluster-size approaching that for bulk [304]. In general, the experimental results confirm the open-shell ground state of small palladium particles. Thus, magnetic properties of cluster-size palladium catalysts should be taken into account as specific properties of such particles are considered.

6.3. Adsorption of an atomic hydrogen on palladium clusters

Fundamental size-dependent differences in hydrogen interactions with palladium clusters and surfaces were observed experimentally. It was found that the

kinetics of the chemisorption of the first hydrogen molecule onto Pd_n ($n \leq 25$) varies strongly with cluster-size with relative reactivity of clusters being dependent on the hydrogen pressure [305]. The saturation studies with deuterium showed that the ratio of D-atoms per Pd-atom is about 3 for Pd_4 and about 2.5 for Pd_6 to Pd_8 ; D/Pd ratio tends to decrease with increasing cluster-size but does not approach unity [305]. On the other hand, small palladium clusters with diameter $d \leq 25 \text{ \AA}$ supported on $\gamma\text{-Al}_2\text{O}_3$ do not absorb hydrogen [234,235]. Similarly, no subsurface or dissolved in the bulk states of hydrogen were observed upon hydrogen interaction with the giant ligand-stabilized palladium clusters with five and seven full-shells [237–239]. Owing to the blocking of some of the surface atoms to the ligands, the number of H-atoms adsorbed per surface Pd atom of these clusters was 0.58 and 0.48, respectively, i.e. significantly below the full coverage limit on the bulk surfaces. Not only the amount of the sorbed hydrogen per palladium atom but also kinetics and chemical potentials appeared in these experiments to depend on the cluster-size [236].

Theoretical aspects of the specific catalytic behavior of ultradispersed palladium particles are relatively scantily known. The numerous quantum-chemical calculations of adsorption and catalytic reactions on palladium surfaces performed within the cluster approximation typically applied a model of few metal atom clusters having the bulk volume and surface structures [306–311]. The most important information relevant to cluster-size catalysts, which can be extracted from such calculations, is the strong non-linear size-dependence of adsorption energies obtained for different adsorbates on transition-metal clusters consisting of few metal atoms [145–148,136,137]. This theoretical result is well consistent with the experimental observations that adsorbent-to-palladium interaction strongly depends on the structure and size of metal particles for both gas-phase [305] and supported [312,313] clusters. High-level quantum mechanical simulations of the atomic, molecular and dissociative adsorption on real-life palladium clusters are still relatively rare.

The Monte Carlo calculations of a cluster consisting of 500 atoms with a radius of 1.3 nm [314] predicted an increased capacity of 1.3 H/Pd with the surface sites being occupied first and a subsequent filling of the interior sites. The embedded cluster method showed that

hydrogen atom is localized in tetrahedral binding sites in the palladium clusters with 4, 5 and 9 metal atoms and in octahedral positions in clusters of 6, 7, 8 and 10 atoms with hydrogen adsorption energy tending to decrease with increasing cluster-size [315]. These theoretical results disagree with the experiments [234–236] since both Monte Carlo and embedded atom methods were fit to bulk data. Thus, even qualitatively, the nature of hydrogen interaction with small palladium clusters should be considered from the first principles.

Interactions of an atomic hydrogen with Pd [317], Pd_2 [318] and Pd_3 [319] clusters were studied by Balasubramanian and co-workers using complete active space multiconfiguration self-consistent field (CAS-MCSCF) followed by multireference CI calculations (MRSDCI). The ground state for all clusters was found to be doublet with the hydrogen binding energy of 2.4, 3.0 and 3.1 eV, Pd–H bond length of 1.54, 1.60 and 1.75 \AA , respectively, and optimized Pd–Pd distances of 2.86 (Pd_2H) and 2.59 \AA (Pd_3H). Only highly symmetric bridge and three-center hydrogen coordinations on Pd_2 and Pd_3 clusters, respectively, were considered in these works. Hydrogen interaction with Pd_{13} clusters was studied using a self-consistent density-functional scheme with focus on the cubo-octahedral Pd_{13}H_n ($n = 1, 6, 8, \text{ and } 14$) clusters [311]. Two stable sites for hydrogen adsorption (slightly inside the square face and in the surface three-fold position of the triangular face) were found in this study and compared with bulk PdH. Hydrogen bonding in Pd_{13}H_8 cluster appeared to be stronger for the icosahedral configuration than for the octahedral one.

Our preliminary B3LYP results (without frequency calculations) on Pd_nH ($n \leq 6$) clusters [320] show that, as in the case of bulk surfaces, hydrogen prefers surface three-fold coordination position. The binding energy calculated with respect to the lowest (triplet) state of the clusters is by few kcal/mol higher than that on the bulk Pd(1 1 1) at the full coverage. It oscillates with the cluster-size and the range of changes narrows with increase of the hydrogen coordination number. This is in variance with the B3LYP results for atomic sulfur and chlorine interactions with the same clusters [321], showing that the adsorption energies vary in a monotonous way as the number of palladium atoms increases and converge rapidly towards limiting values, which are significantly lower than those calculated for the bulk Pd(1 1 1) surface [93]. It is interesting

to note here that, as opposed to the bulk surface, on Pd₄ cluster one adsorbed S-atom increases, while one co-adsorbed Cl-atom decreases the hydrogen adsorption energies compared to the clean cluster [218].

6.4. Hydrogen dissociation on small palladium clusters

More attention was paid to the hydrogen dissociation on palladium clusters. The high-level calculations on Pd_n/H₂ systems are restricted to $n \leq 4$ [145,193,194,192,197,261–265]. In some of these works [145,193,194] palladium clusters served as a model of a bulk surface; they had closed-shell electronic structure and their geometry was fixed at the fcc palladium crystalline lattice. In the other studies [196,197,199] the cluster geometry was optimized for several highly symmetric adsorption positions. Full optimization of the geometry was done for Pd_n/H₂ systems with $n \leq 4$ in the DFT studies at the B3LYP level of theory for the several most stable stationary states [261–263]. A rich variety of reaction pathways and local minima including those associated with weak interactions were studied using the same method and for the same clusters in [265,323]. With increasing cluster-size the number of nearly degenerated stable structures increases steeply, however, depending on the coordination number of hydrogen atoms, all possible structures can be divided into several groups with similar geometries and energies. The computational results for representative dihydrogenated palladium clusters for each group are summarized in Table 6.

In the Pd–H₂ system both side-on and end-on approach modes lead to the formation of weak complexes [192,197,199,261,264,265]. While there is an experimental evidence of the side-on hydrogen capture by isolated palladium atom in noble gas matrixes at 12 K [192], frequency calculations point out that the linear Pd–H–H configuration is not a real minimum and forces will turn it into the most stable in the system side-on mode. The dissociation of the H–H bond in the last configuration is energetically not favorable—the resulting complex lies 0.20 eV higher than the most stable structure. The linear H–Pd–H state is extremely unstable with respect to H₂ abstraction.

Due to the open-shell electronic structure of larger palladium clusters in the ground state, the multiplicity considerations become very important in the Pd_n–H₂












interactions for $n \geq 2$. Depending on the hydrogen adsorption energy and the singlet–triplet separation energy of clusters, a singlet or a triplet state of the system can be more stable. For the clusters at hand the high energy for the atomic hydrogen adsorption favors the singlet ground state of the systems [261–263,265] while the triplet state is the most stable for weakly bound non-dissociated complexes [323]. As in the case of bulk surfaces, some of the reaction pathways have no or very low activation barriers to the hydrogen dissociation.

Palladium dimer forms very stable dissociative structure with two H-atoms in the bridge positions (Table 6). Hydrogen adsorption is accompanied by strong changes in the geometric and electronic structures of the cluster: the Pd–Pd distance increases by 0.11 Å and the system switches to the closed-shell electronic structure. The ground state configuration is not planar with the H–H bond being 0.09 Å above the Pd–Pd bond. This structure can be achieved in the side-on and end-on H₂ approach modes towards a Pd–Pd bond with the former reaction pathway being non-activated on both singlet and triplet PES. The ground state final configuration and the most favorable reaction pathway differ from those for other transition-metals and are determined by the specific electronic structure of palladium atoms, i.e. by their near empty 5s orbitals [261]. As it was discussed in connection with hydrogen dissociation on bulk surfaces, non-activated dissociation becomes possible owing to the effective donation from the occupied H₂σ-MO to the lowest empty σ_g orbital of the cluster. In the final state both the H–Pd–Pd bonding and antibonding orbitals again have much contribution from the diffusive Pd 5s component that favors the bridge position rather than the localized metal sites. In the ground open-shell electronic state of the cluster Pd 5s orbitals are half-occupied and it results in the extremely high activation barrier to the hydrogen dissociation of 3.68 eV on the triplet PES. The resulting end-structure, which involves electronic excitation to the σ* orbital, destabilizes both the Pd–Pd and Pd–H interactions and therefore, it lies 2.47 eV higher than that in the singlet state and is extremely unstable with respect to H₂ abstraction.

The most stable structure localized in the Pd₃–H₂ system [262] corresponds to the adsorption of one hydrogen atom in the three-fold and one in the

Table 6

Adsorption energies for several stable states in $\text{Pd}_n + \text{H}_2$ ($n = 1-4$) with respect to the system's ground state ($E_{\text{ad.}}$, eV) calculated at the B3LYP/LANL2DZ level, corresponding H–H ($d_{\text{H-H}}$, Å) and Pd–H distances ($d_{\text{Pd-H}}$, Å) and activation barriers on the singlet (E^\ddagger (S), eV) and triplet (E^\ddagger (T), eV) PES cross-sections

n	Structure	Symmetry	State	$E_{\text{ad.}}$	$d_{\text{H-H}}$	$d_{\text{Pd-H}}^{\text{a}}$	E^\ddagger (S)	E^\ddagger (T)
1 ^b		C_{2v}	1A_1	0.84	0.88	1.68		
		C_{2v}	1A_1	0.64	1.74	1.52		
		D_h	$^1\Sigma_g$	-1.47	3.28	1.64		
2 ^b		C_{2v}	1A_1	1.73	1.94	1.67	0	0
3 ^c		C_s	$^1A'$	1.41	2.69	1.71	0	
		C_s	$^1A'$	1.39	2.04	1.65		
		C_s	$^1A'$	1.36	1.62	1.78	0	0.1
		C_s	$^3A'$	0.47 ^d	0.81	1.85	0.28 ^e	0.18 ^e
4 ^b		C_{2v}	1A_1	1.06	3.40	1.64	0.45	0.85
		C_{2v}	1A_1	1.00	2.20	1.70	0.24	0.39
		C_s	$^3A''$	0.38	0.83	1.79	0.18 ^e ; 0.26 ^f	0.46 ^e ; 0.52 ^f

^a The shortest Pd–H distances are presented for non-symmetric bonds.

^b From [265,323].

^c From [262,263].

^d Triple-zeta basis set.

^e Activation barrier for on-top hydrogen dissociation with respect to the precursor state.

^f The same for “steering” mechanism (see text for details).

bridge positions with trans orientation to one another (Table 6). The non-planar $\text{Pd}_3\text{-H}_2$ complex with two bridge-bound hydrogen atoms in *cis*-configuration and the $\text{Pd}_3\text{-H}_2$ complex with hydrogen atoms in a double three-fold site are located within 0.1 eV over the ground state with the isomerization barrier of about 0.17 eV. The side-on approach of the hydrogen

molecule towards one of the Pd–Pd bonds leads to the hydrogen dissociation. Depending on the orientation of H–H axis with respect to Pd_3 plane the first or the last final configuration can be obtained without an activation barrier on the singlet PES while for the triplet state small activation barriers present on the potential curves. The final structure in the triplet

state is only 1.23 eV less stable than the ground state complex and the hydrogen dissociation on the Pd₃ triplet becomes both thermodynamically and kinetically allowed. Such dramatic difference in the activity of Pd₂ and Pd₃ triplets is due to the shift of Pd 5s electronic density in the latter cluster towards third palladium atom, which does not participate directly in the interaction with hydrogen.

The dissociated structure with two hydrogen atoms in the bridge coordination positions on the opposite Pd–Pd bonds appears to be the most stable for the palladium tetramer [265,263]. While this adsorption position differ from the most stable sites on the bulk surfaces, the obtained value of $E_{ad.}=1.06$ eV is very close to that on the Pd(1 1 1) (0.99 eV [200,201]). The adsorption energy of the three-fold coordination is slightly smaller for this cluster (Table 6). Among the large variety of the reaction pathways considered for hydrogen dissociation on the Pd₄ cluster in no case the non-activated reaction profile was found for both singlet and triplet states [323]. This is in contrast to the smaller clusters, as well as to bulk surfaces. In variance to the bulk surfaces, the main reason for appearance of an activation barrier for hydrogen dissociation on palladium tetramer arises from the reconstruction of cluster geometry along the reaction path. The energy gain for an atomic hydrogen adsorption on the Pd₄ triplet is 0.67 eV smaller than that for the end complex in the singlet state. The size dependence of the stability of Pd_nH₂ complexes agrees qualitatively with the experimentally observed reactivity of small palladium clusters [305], i.e. the palladium dimer was found to form the most stable dihydrogenated complex.

Finally, let us consider the weakly bound dihydrogenated complexes formed by palladium trimer and tetramer. A state of the molecular adsorption is formed spontaneously and is characterized by soft relaxation of the reactants geometry. It was localized for the side-on hydrogen capture by one of the metal atoms in Pd_n clusters with the H₂ center of mass being notably shifted from the main symmetry axis and had the lowest triplet state. The local geometry of the pre-dissociated complexes (Table 6) is very similar to that obtained for the precursor state on the bulk surfaces (Table 5) and their stability is close to that on the crystallographically “open” Pd(1 1 0) plane. Similarly to the bulk surfaces, this precursor state presents the most attractive position for the capping of a hy-

drogen molecule far from the cluster and precedes the hydrogen dissociation in both singlet and triplet states. As on the bulk surfaces, steering of the activated hydrogen molecule with the H–H axis perpendicular to the symmetry plane leads to its dissociation near the center of the Pd–Pd bond. However, on the clusters there is yet another transition state for the dissociation, in which one of hydrogen atoms moves towards a bridge site and another one remains in the one-fold position. The latter reaction pathway is energetically more favorable than the former one, however, even in this case, the activation barrier to the hydrogen dissociation on small clusters is higher than that on the bulk surfaces (compare Tables 5 and 6).

Thus, the only stable complex formed by palladium trimers and tetramers in the ground state without a barrier involves activated molecularly adsorbed hydrogen. Since the ground state of the Pd_n–H₂ system with $n \geq 2$ in the initial state is triplet and in the final state is singlet, the hydrogen dissociation on palladium clusters is connected with intersystem crossing. It leads to an additional increase in the activation energy for the dissociation and causes a farther stabilization of the hydrogen precursor state as compared to the single crystal palladium surfaces. Moreover, it was found that dihydrogenated Pd₃ and Pd₄ clusters can accept additional hydrogen molecules to their unsaturated metal atoms with the formation of hydrogenated complexes, in which the first hydrogen molecule is dissociated and the others are bound molecularly [263]. The adsorption energies for the bonding of the additional hydrogen molecules to the dihydrogenated palladium clusters fall within the range between 0.39 and 0.57 eV, i.e. such complexes are fairly stable. However, the unfavorable entropy contribution for their formations increases rapidly with increasing temperature and hydrogen loading. This may be the reason why the extra adsorption was observed experimentally for deuterium and not for hydrogen [305]. The high stability of the pre-dissociated state of the adsorbed hydrogen presents, probably, the main characteristic feature of hydrogen interactions with small palladium clusters.

6.5. Supported palladium clusters

Supported and bimetallic palladium clusters and their reactivity are of special importance for practical applications and for understanding of catalytic

processes from the fundamental point of view. It is well known that the nanometer-sized supported metal clusters behave differently than bare clusters and extended surfaces. For example, activated carbon, which can be expected to induce only minor changes in the charge distribution in supported palladium particles, leads to expansion of the Pd lattice in the supported catalysts and causes significant suppression of hydrogen adsorption and absorption while heat of adsorption is close to that on bulk surfaces and bare clusters [324]. Small palladium clusters with diameter $d \leq 25 \text{ \AA}$ supported on $\gamma\text{-Al}_2\text{O}_3$ do not absorb hydrogen [234–236]. Sorption–desorption isotherms in the $\text{H}_2\text{-Pd}$ -support systems often show the existence of a hysteresis [325,326]. For nano-scale Pd clusters with relatively weak intermetallic interactions both geometric and electronic structures changes as a result of the interaction with support. These alterations are caused by two main reasons: possible charging and formation of new chemical bonds between palladium nano-particles and a support. Both these factors significantly affect the catalytic properties.

The high-level theoretical study of the structure and reactivity of supported transition-metal clusters is still at the very beginning owing to the lack of accurate experimental information about the structural aspects of the catalyst–support interface and to computational difficulties connected with a large size of a model metal–support system. The main attention in the modern literature is paid to the understanding of the nature of the palladium–support interactions and corresponding perturbations in the catalyst electronic structure. As a probe of the surface electronic structure of mono- and bimetallic, supported or electrochemically activated catalysts the carbon monoxide chemisorption is frequently used in both experimental [327,328] and theoretical [316,329–333] investigations since, according to the widely accepted Blyholder model [334], the nature of CO interaction with transition-metal surfaces is determined by two main components: a σ -bond formed between the CO carbon atom and metal surface mainly due to the electron transfer from the adsorbent to the surface and the partial filling of the CO π^* -MO due to the back-donation from the metal d-orbitals. Although, the model was shown to be significantly simplified [335–337], it enables to estimate the acceptor and donor properties independently at the same extend

as metal–C and C–O bonds may be characterized. These investigations showed that, due to its specific electronic structure, palladium is very sensitive to the nature and structure of the second constituent of a catalyst and a number of elegant studies were reported recently in this field [338–345]. The theory of hydrogen adsorption and, especially, hydrogen dissociation on supported palladium clusters is not far enough advanced to offer the subject for critical analysis. The systematic theoretical studies of metal atoms and clusters interacting with common oxide supports are conducted by Pacchioni and co-workers and Illas and co-workers. Here the recent theoretical data on the support-induced alterations in geometric and electronic structure of palladium atom and clusters will be briefly considered mainly on the ground of the published results of these two groups. A detailed discussion of the subject one can find in several recent books and reviews [346–349]. The main part of such studies was performed using DFT methods within cluster model approximation. For oxide supports like SiO_2 and TiO_2 [350] it was found that the application of rather small model clusters is enough in order to represent the coordination site of the support.

The EXAFS structural analysis indicates that the small metal particles, anchored on an alkaline support are in contact only with the oxide ions of the support, primarily due to a Coulomb attraction between metal particle and support oxygen ions [351]. The IR, XPS, and shape resonance data show that the interaction between the metal and support leads to a shift in the energy of the metal valence orbitals. As the alkalinity of the support increases, there is a decrease in the metal ionization potential and the difference in energy between metal–H antibonding orbital and the Fermi level decreases [351]. The Hartree–Fock and gradient-corrected DFT cluster calculations reveal that the bonding of a single palladium atom with the non-defective sites of the SiO_2 surface is very weak ($\sim 0.22 \text{ eV}$), sticking of the atoms occurs only at the defect sites [352]. The most attractive sites for the adsorption of Pd atom are non-bridging oxygen atoms with adsorption energy of 2.51–2.85 eV at the B3LYP level of theory in comparison to 2.16–2.27 eV for adsorption on defect Si-bonds. Palladium atoms connected to oxygen defect sites keep significant (0.17–0.25) positive charge while on different Si-centers charges on the supported

Pd atoms range from -0.38 to -0.89 . On the oxygen adsorption sites palladium atom interacts simultaneously with two or more surface oxygens with the shortest Pd–O bond length of 2.03 – 2.09 Å. The SiO_2 surface was modeled in this study by Si_1O_n ($n = 3, 4$) and Si_2O_m ($m = 6, 7$) clusters with structures derived from that of α -quartz and with broken bonds saturated by H-atoms.

The adsorption of isolated Pd atoms and Pd dimers on the regular $\text{TiO}_2(110)$ surface was studied by gradient-corrected DFT methods with the non-defective rutile (110) surface being modeled by neutral stoichiometric clusters $(\text{TiO}_2)_n$ ($n = 2$ – 15) embedded in finite arrays of point charges and total ion model potentials or by periodic slab [350]. It was found that on the rutile surface Pd forms more covalent polar bonds with the net positive charge on Pd of not more than 0.3 . On the relaxed rutile surface palladium adsorption leads to changes in the surface bonds that indicates possible surface reconstruction induced by adsorbed atoms. In variance to the silica, also the regular rutile surface shows strong adhesion ability at both Ti and O sites in accordance with the experimentally observed random distribution of ultrasmall palladium particles over the $\text{TiO}_2(110)$ surface [353]. At low coverage the preferential adsorption position for Pd atom was found to be on the two-fold coordinated protruding oxygens with the adsorption energy of 1.03 eV while the bond strength of 0.43 – 0.64 eV was found along the Ti rows. However, comparison of periodic supercell and cluster model results allowed the authors to suggest that the most stable site for palladium adsorption changes with increasing coverage and at coverage of 0.25 ML palladium atoms prefer the adsorption sited on Ti rows. This is at variance with the results for adsorption of Cu, Ag and Au atoms on the same surface where the O-sites were found to be much more stable [354]. The authors attribute this fact to a mixing of the 4d levels on Pd with the 3d empty states of the Ti cations, which leads to the formation of a relatively strong bond with covalent polar character while Cu, Ag, and Au have no possibility to form such hybrid levels because they have completely filled nd shells and a partially occupied $(n + 1)s$ level. While the number of surface position available for adhesion of palladium on rutile is much larger than that on silica, the adsorption energy on rutile is significantly lower that is again in line with

high mobility of small palladium particles on the $\text{TiO}_2(110)$ surface found experimentally [353].

In agreement with STM data [355] the Pd_2 cluster prefers to adsorb on the five-coordinated Ti sites. Pd dimers adsorbed on the rutile surface lose most of the Pd–Pd interaction due to the relatively strong bond with the substrate. In the most stable position each palladium atom forms four Pd–O bonds with bond length of 2.47 Å and one Pd–Ti bond with bond length of 2.80 Å. The Pd–Pd distance elongates to 2.93 Å (in comparison with 2.53 and 2.76 Å in the isolated dimer in the ground triplet and excited singlet states, respectively) and becomes close to the value required for pseudo-morphic growth (2.95 Å). The palladium-support interaction is essentially covalent with Pd net charge of $+0.17$. The adsorption position in which palladium dimer is bridging two O-atoms is only 0.07 eV per Pd atom less stable than the energetically preferential adsorption site. In this latter case palladium atoms keep larger deficit of electron density ($+0.33$); the Pd–O bond length is 2.21 Å and Pd–Pd distance (2.79 Å) is only slightly longer than that in the Pd_2 cluster in the singlet state. The electronic configuration of adsorbed palladium atoms ($4d^{9.5}sp^{0.3}$) is about the same for all coordination positions. Adsorption of a CO molecule on Pd dimers shows that, regardless of the site where the Pd atom sits, the supported clusters form significantly (by more than 1 eV) less stable carbonyls than free clusters. This effect is due to the partial occupation of diffuse 5sp orbitals and therefore, to increasing Pauli repulsion contribution to the CO–Pd bonding while the ability of the supported metal to donate electrons to CO remains very similar to that of the free cluster.

Adsorption of Pd_n ($n = 1$ – 5) clusters on $\text{MgO}(100)$ surface was investigated using cluster and slab models and a variety of ab initio and DFT techniques [356,364,365,358]. Palladium atoms were found to favor adsorption sites on top of oxygen centers of the regular $\text{MgO}(001)$ substrate at coverage $\theta = 0.25$ within periodic model [365] and at zero-coverage limit within cluster model [356–359] with the same adsorption energy of 0.81 eV and a distance of 2.1 – 2.2 Å [365,357,359,358]. However, the atomic adsorption of palladium atom on neutral and singly positively charged oxygen vacancies of defect $\text{MgO}(100)$ surfaces is significantly (by 1.2 – 2.5 eV) stronger and is accompanied by extremely large reorganization of

Pd electronic configuration ($4d^{9.4}s^{1.7}$ and $4d^{9.4}s^{1.2}$ for the above sites, respectively in comparison with $4d^{9.5}s^{0.7}$ for the regular surface¹) [360]. These defect sites seem to serve as a nucleation centers for the growth of palladium nano-particles during the catalyst preparation due to the relatively high mobility of palladium atoms on the regular MgO surface (even though the highest adsorption energy of 1.35 eV estimated by relativistic DFT calculations is considered). Nevertheless, adhesion of larger (Pd_{2-5}) clusters was studied only on the regular MgO(100) surface [299,361,362,359,364]. It was found that the clusters adsorb in proximity of oxygen centers and tend to form spatial 3D structures while pseudo-morphic 2D configurations are less stable. This is in line with molecular dynamics simulations of the structure of palladium clusters deposited on the MgO(001) surface [363], which allow one to expect the formation of monolayers far from the equilibrium conditions; at higher temperatures as well as in the case of the deposition of 3D aggregates palladium clusters evolve to form 3D structures while the initial shape of clusters is strongly modified. The adsorption was found to induce the spin quenching from triplet to singlet for palladium dimer while both spatial and planar Pd tetramers adsorbed on the regular MgO(100) surface are triplets in the ground state. The interaction with the support causes a weakening of the metal–metal bonds between palladium atoms directly involved in the interaction with the support, which results in an elongation of the Pd–Pd distances within 2D clusters. Contrary, the second-layer palladium atoms are extremely strongly bound to the first-layer ones that causes suppression of Pd–MgO interactions and notable shortening of all Pd–Pd bonds. The CO adsorption on the supported Pd atom is stronger than that on the free atom, whereas characteristics of the Pd–C and C–O bonds are very similar. The support-induced alterations in the Pd–CO interaction tend to increase

¹ Presented orbital occupations are based on the Mulliken population analysis and have to be analyzed with care due to the known limitations of the method. They probably correctly describe the qualitative trends in the electronic structure of adsorbed palladium atoms, but not the net atomic charge. No significant charge transfer between adsorbed Pd atom and MgO surface was reflected by CO adsorption; the palladium–substrate bonding is attributed to polarization of the adsorbed atoms in the electrostatic field of the ionic substrate and to some covalent contributions.

with the cluster-size and even the preferential adsorption site on the square-planar Pd_4 changes from hollow on the free cluster to top on the supported one. The Pauli repulsion between Pd 5sp orbitals and incoming CO molecule are mentioned as the key factor determining these alterations.

Such a brief look at the best theoretical studies on supported palladium clusters shows that palladium particles deposited on oxide supports tend to form strong bonds with the surface O-atoms and demonstrate significant reorganizations in the metal geometric and electronic structures, which are strongly dependent on the composition and surface structure of the support. Clearly, these support-induced perturbations may be sufficient to change the order of stability of various adsorption sites on the metal cluster, their reactivity towards hydrogen bonding and activation and nature of palladium–hydrogen interactions. Moreover, the adsorption of hydrogen, in turn, can affect the surface composition and geometry [366]. Due to a hydrogen spillover palladium effectively promotes the reduction of oxide support [367,368] that provides an additional source of modifications in palladium–support interaction and reactivity of resulting catalysts. Practically, such factors inherent for nanometer chemistry as reactant supply via the support, interplay of the reaction kinetics on different facets of supported particles, and oscillation and chaos on the nanometer scale can add complicity to the kinetics of catalytic reactions on nano-sized metal particles, especially in the case of rapid catalytic reactions occurring far from the adsorption–desorption equilibrium [369]. Thus, in spite of the wide application of supported palladium clusters, the molecular details of hydrogen–Pd–support interactions are still not clearly understood. This is the field, in which combined experimental and theoretical studies should answer the fundamental questions of the mechanisms of catalytic action and open the real way for catalyst design.

7. Conclusions and perspectives

This review was aimed to analyze the current understanding of the catalytic sites on transition-metal surfaces and to follow the relationship between geometric and electronic structures and adsorptive properties in catalysis based on the recent theoretical and

experimental studies of the hydrogen interactions with the single crystal bulk palladium surfaces and with small palladium clusters as a model system. It is shown that the local electronic structure and the geometric configuration of surface catalytic centers vary for different single crystal bulk surfaces and clusters, but these changes have only limited influence on the energetics of the atomic hydrogen adsorption in the most stable coordination sites. In contrast, atomic adsorbates in the low-coordinated positions are essentially sensitive to such changes. As a sequence, the reactivity and the mobility of surface H-atoms increases in the following order: close-packed surfaces < “open” surfaces < small clusters. The adsorbent–surface interactions are shown to have essentially local nature with the electronic and geometric structures of an adsorbed hydrogen atom being solely determined by its coordination number. The specific surface structure manifests itself in the long-range adsorbent-induced changes in interatomic bonds and, as a sequence, in the total adsorption energetics.

The main common feature of the considered palladium surfaces and clusters is that all of them have at least one reaction path for the hydrogen dissociation without or with very low activation barrier. However, this holds only for few pathways; in particular, to be able to dissociate the molecule should reach the surface with an appropriate orientation. The main part of hydrogen molecules with low kinetic energy are capped by palladium surfaces and clusters with formation of the weakly bound molecularly adsorbed states. Both thermodynamic and kinetic stability of such complexes tends to increase then moving from close-packed to more crystallographically “open” palladium crystal faces and from the bulk surfaces to clusters. The unique feature of small palladium clusters — their ground state magnetism affects significantly the dynamics of dissociative adsorption and leads to additional stabilization of the pre-dissociated form of hydrogen.

The most important issue addressed by the theoretical chemistry applied to catalysis is the mechanism of catalytic reactions. Significant progress in this field was achieved in the last decade. However, this subject was not considered here by the following main reasons. First, several very informative reviews on the mechanism of CO hydrogenation over palladium were published recently [370,371]. The current un-

derstanding of the mechanism of olefin hydrogenation is described exhaustively in [295,372,373]. Second, the high-level theoretical study of the mechanisms of catalytic reactions is still at the initial stage and the main part of the available results is restricted to the (111) crystal plane of the adsorbent. Finally, taking into account the pronounced influence of the surface geometry on the catalyst activity and selectivity, on the one hand, and on the weakly bound atomic and especially molecular states of the adsorbed hydrogen, on the other hand, it would be reasonable to examine the role of such species in hydrogenation processes. This assumption agrees with the experimental observations that the adsorbed hydrogen participating in the hydrogenation of olefins is rather weakly bound to the surface [374] and that the surface state of an adsorbed hydrogen determines activity and selectivity of transition-metal catalysts in hydrogenation of unsaturated C–C bonds [375–378]. However, to the best of our knowledge, in all the theoretical studies only the atomically adsorbed hydrogen in the ground state was considered as a hydrogenating agent while the participation of the π -bound state of ethylene in the process was confirmed for high surface coverages [295,372,373], in accordance with the experimental results [379–382]. Thus, mechanisms of these reactions need more attention.

The theoretical tools for such demanding task as the modeling of adsorption and reactions on transition-metal surfaces are still under development, but modern DFT techniques based on the B3LYP exchange–correlation potential (within the cluster model) and especially, GGA approximation (within the periodic slab model) become robust and efficient methods for detailed qualitative and quantitative analysis of such surface phenomena. Considering the palladium–hydrogen interaction as a model system, the detailed analysis of the recent publications allows one to see some general features of modern quantum chemical investigations on surface–adsorbate interactions.

- Due to high theoretical level of approximations, calculated geometries and energetics of adsorption–absorption structures agree quantitatively with experimental data.
- Relatively complicated hypotheses derived from experimental results can now be modeled directly and not only qualitatively estimated.

- Much more attention is paid to adsorbent-induced changes in geometric and electronic structure of surfaces and adsorption sites.
- Significant attention is paid to weakly bound physically and chemically adsorbed states which, according to the recent experimental data, are often of paramount importance in catalytic reactions.
- Molecular orientation is widely considered as a controlling process in adsorption dynamics.

Continuing theoretical and computational advances in conjunction with development in the experimental techniques and in the material science makes it possible to solve in the nearest future the tricky problem of the mechanisms of hydrogenation and to be able to design catalytic particles and surfaces with desirable properties.

Acknowledgements

The author is indebted to Moshe Sheintuch and Ernst D. German for their invaluable help and advises concerning the matter of the paper. I would like to thank Werner Kutzelnigg, Jose A. Rodriguez, and Djamaladdin G. Musaev for helpful discussion and Milan Kralik for encouraging me to write this paper. I acknowledge receiving reprints and preprints suitable for the paper from W. Kutzelnigg, H. P. Toulhoat, G. Tréglia, and D. G. Musaev. This work was supported by the Center for Absorption in Science, Ministry of Immigrant Absorption, State of Israel.

References

- [1] A.A. Balandin, *Z. Phys. Chem.* B3 (1929) 167.
- [2] A.A. Balandin, *J. Russian Phys.-Chem. Soc.* 61 (1929) 909.
- [3] A.A. Balandin, *J. Russ. Phys.-Chem. Soc.* 62 (1930) 703 (in Russian).
- [4] A.A. Balandin, *Catalysis and Chemical Kinetics*. Academic Press, NY, 1964.
- [5] H.S. Taylor, *Proc. R. Soc. A* 108 (1925) 105.
- [6] H.S. Taylor, *Phys. Chem.* 30 (1926) 145.
- [7] Z. Karpinski, *Adv. Catal.* 37 (1990) 45.
- [8] R.C. Baetzold, *J. Chem. Phys.* 55 (1971) 4355.
- [9] R.C. Baetzold, *J. Chem. Phys.* 55 (1971) 4363.
- [10] R.C. Baetzold, *J. Chem. Phys.* 62 (1975) 1513.
- [11] E.R. Davidson, *Chem. Rev.* 91 (1991) 649.
- [12] T. Ziegler, *Chem. Rev.* 91 (1991) 651.
- [13] R.F. Nalewajski (Ed.), *Topics in Current Chemistry*, Vols. 180–183, Springer, Berlin, 1996.
- [14] J. Labanowski, J. Andzelm (Eds.), *Density Functional Methods in Chemistry*, Springer, Heidelberg, 1991.
- [15] R.G. Parr, W. Yang (Eds.), *Density Functional Theory of Atoms and Molecules*, Oxford University Press, New York, 1988.
- [16] A. Dedieu, *Chem. Rev.* 100 (2000) 543.
- [17] A.M. Dirac, *Proc. R. Soc. London A* 123 (1929) 714.
- [18] I.N. Levine, *Quantum Chemistry*, Prentice-Hall, New Jersey, 1991.
- [19] A. Szabo, N.S. Ostlund, *Modern Quantum Chemistry: Introduction to Advanced Electronic Structure Theory*, McGraw-Hill, New York, 1989.
- [20] R. McWeeny, *Methods of Molecular Quantum Mechanics*, Academic Press, London, 1989.
- [21] M. Head-Gordon, *J. Phys. Chem.* 100 (1996) 13213.
- [22] J.K. Labanowski, J.W. Andzelm (Eds.), *Density Functional Methods in Chemistry*, Springer, 1991.
- [23] D.P. Chong (Ed.), *Recent advances in density functional methods. Part 1*. World Scientific, Singapore, 1995.
- [24] B.B. Laird, R.B. Ross, T. Ziegler, *Chemical Applications of Density-Functional Theory*, ACS, Washington, DC, 1996.
- [25] Á. Nagy, *Phys. Rep.* 298 (1998) 1.
- [26] W. Koch, M.C. Holthausen, *A Chemist's guide to density functional theory*, Wiley, New York, 2000.
- [27] R.A. van Santen, M. Neurock, *Cat. Rev.-Sci. Eng.* 37 (1995) 557.
- [28] S. Yoshida, S. Sakaki, H. Kobayashi, *Electronic Processes in Catalysis: A Quantum Chemical Approach to Catalysis*, VCH Publications, New York, 1994.
- [29] L. Szasz, *Pseudo-Potential Theory of Atoms and Molecules*, Wiley, New York, 1986.
- [30] M. Krauss, W.J. Stevens, *Ann. Rev. Phys. Chem.* 35 (1984) 357.
- [31] P. Durand, J.P. Malrieu, *Adv. Chem. Phys.* 67 (1987) 321.
- [32] J.A. Pople, *Rev. Mod. Phys.* 71 (1999) 1267.
- [33] P. Hohenberg, W. Kohn, *Phys. Rev. B* 136 (1964) 864.
- [34] W. Kohn, L.J. Sham, *Phys. Rev.* 140A (1965) 1133.
- [35] G. Frenking, I. Antes, M. Boehme, S. Dapprich, A.W. Ehlers, V. Jonas, A. Neuhaus, M. Otto, R. Stegmann, A. Veldkamp, S.F. Vyboishchikov, in: K.B. Lipkowitzand, D.B. Boyd (Eds.), *Rev. Comp. Chem.*, Vol. 8, VCH Publications, New York, 1996, p. 63.
- [36] M. Torrent, M. Solá, G. Frenking, *Chem. Rev.* 100 (2000) 439.
- [37] G. Frenking, N. Fröhlich, *Chem. Rev.* 1000 (2000) 717.
- [38] H. Chermette, *J. Comp. Chem.* 20 (1999) 129.
- [39] P. Geerlings, F. De Proft, W. Langenaeker, *Adv. Quant. Chem.* 33 (1998) 303.
- [40] A.D. Becke, *Phys. Rev. A* 38 (1988) 3098.
- [41] A.D. Becke, *J. Chem. Phys.* 98 (1993) 1372.
- [42] A.D. Becke, *J. Chem. Phys.* 98 (1993) 5648.
- [43] C. Lee, W. Yang, R.G. Parr, *Phys. Rev. B* 37 (1988) 785.
- [44] J.P. Perdue, *Phys. Rev. B* 33 (1986) 8822.
- [45] J.P. Perdue, Y. Wang, *Phys. Rev. B* 45 (1991) 13244.
- [46] A.G. Zacarias, M. Castro, L.M. Tour, J.M. Seminario, *J. Phys. Chem. A* 103 (1999) 7692.
- [47] W. Thiel, *Adv. Chem. Phys.* 93 (1996) 703.

- [48] G. A. Segal (Ed.), *Semiempirical Methods of Electronic Structure Calculation*. Part A. Plenum Press, New York, 1977.
- [49] J.J.P. Steward, *Semiempirical molecular orbital methods*, in: K.B. Lipkowitz, D.B. Boyd (Eds.), *Reviews in Computational Chemistry*, 1990, p. 45.
- [50] W. Thiel, *J. Mol. Struct. Theochem.* 398/399 (1997) 1.
- [51] M. Malagoli, W. Thiel, *Chem. Phys.* 206 (1996) 73.
- [52] W. Thiel, A.A. Voityuk, *J. Phys. Chem.* 100 (1996) 616.
- [53] T.R. Cundari, J. Deng, *Chem. Inf. Comput. Sci.* 39 (1999) 376.
- [54] M. Bräuer, M. Kunert, E. Dinjus, M. Klußmann, M. Döring, H. Görls, E. Anders, *J. Mol. Struct. Theochem.* 505 (2000) 289.
- [55] V. Gineityte, *J. Mol. Struct. Theochem.* 491 (1999) 205.
- [56] R. Stowasser, R. Hoffmann, *J. Am. Chem. Soc.* 121 (1999) 3414.
- [57] F. Driessler, W. Kutzelnigg, *Theor. Chim. Acta* 43 (1976) 1.
- [58] F. Driessler, W. Kutzelnigg, *Theor. Chim. Acta* 43 (1977) 307.
- [59] R. Hoffmann, *Solids and Surfaces*, VCM Publications, New York, 1988.
- [60] A.B. Anderson, R. Hoffmann, *J. Chem. Phys.* 60 (1974) 4271.
- [61] A.B. Anderson, *J. Chem. Phys.* 62 (1975) 1187.
- [62] A.B. Anderson, R.W. Grimes, S.Y. Hong, *J. Chem. Phys.* 91 (1987) 4245.
- [63] H.F. Ades, A.L. Companion, K.R. Subbaswamy, *J. Phys. Chem.* 95 (1991) 6502.
- [64] T. Koerts, R.A. van Santen, *J. Mol. Catal.* 70 (1991) 119.
- [65] A.B. Anderson, *J. Mol. Catal.* 54 (1989) 281.
- [66] A.B. Anderson, M.K. Awad, *J. Am. Chem. Soc.* 107 (1985) 7854.
- [67] A.B. Anderson, Y. Kim, D.W. Eving, R.K. Grasselli, M. Tenhover, *Surf. Sci.* 134 (1983) 237.
- [68] A.B. Anderson, M.R. McDevitt, F.L. Urbach, *Surf. Sci.* 146 (1984) 80.
- [69] A.B. Anderson, E. Grantscharova, *J. Phys. Chem.* 99 (1995) 9143, and many other papers of A.B. Anderson and co-workers.
- [70] C.M. Goringe, D.R. Bowler, E. Hernandez, *Rep. Prog. Phys.* 60 (1997) 1447.
- [71] G. Fabricius, A.M. Llois, M. Weissmann, M.A. Khan, *Phys. Rev. B* 49 (1994) 2121.
- [72] A. Vega, J. Dorantes-Davila, L.C. Balbas, G.M. Pastor, *Phys. Rev. B* 47 (1993) 4742.
- [73] T.J. Raeker, A.E. DePristo, *Phys. Rev. B* 39 (1989) 99676.
- [74] M.I. Baskes, M.S. Daw, S.M. Foiles, *Mater. Res. Soc. Symp. Proc.* 141 (1989) 31, (*At. Scale Calc. Mater. Sci.*).
- [75] A.P. Horsfi, A.M. Bratkovsky, *J. Phys.: Condens. Matter* 12 (2000) R1.
- [76] R. Car, M. Parrinello, *Phys. Rev. Lett.* 55 (1985) 2471.
- [77] E. Shustorovich (Ed.), *Metal-Surface Reaction Energetics: Theory and Applications to Heterogeneous Catalysis, Chemisorption, and Surface Diffusion*, VCH Publications, New York 1991.
- [78] E. Shustorovich, H. Sellers, *Surf. Sci. Rep.* 31 (1998) 1.
- [79] G.M. Zhidomirov, V.B. Kazansky, *Quantum-chemical cluster models of acid–base sites of oxide catalysts*, *Adv. Cat.* 34 (1986) 131.
- [80] C. Minot, A. Markovits, *J. Mol. Struct. (Theochem.)* 424 (1998) 119.
- [81] J.L. Whitten, H. Yang, *Surf. Sci. Rep.* 24 (1996) 55.
- [82] J.N. Murrell, *J. Mol. Struct. Theochem.* 424 (1998) 93.
- [83] M. Heinrichsmeier, A. Fleszar, W. Hanke, A.G. Eguiluz, *Phys. Rev. B* 57 (1998) 14974.
- [84] G.D. Kubiak, *J. Vac. Sci. Technol. A* 5 (1987) 731.
- [85] R. Fischer, S. Schuppler, N. Fischer, T. Fauster, W. Steinmann, *Phys. Rev. Lett.* 70 (1993) 654.
- [86] S. Schuppler, N. Fischer, T. Fauster, W. Steinmann, *Phys. Rev. B* 46 (1992) 13539.
- [87] J. Hölzl, F.K. Schulte, *Solid Surface Physics*, Springer Tracts in Modern Physics, Vol. 85, Springer, Berlin, 1979, p. 1.
- [88] P.D. Johnson, S.L. Hulbert, *Phys. Rev. B* 35 (1987) 9427.
- [89] P. Nordlander, S. Holloway, J.K. Norskov, *Surf. Sci.* 136 (1984) 59.
- [90] S. Sawaya, J. Goniakowski, C. Mottet, A. Saúl, G. Trégliia, *Phys. Rev. B* 56 (1997) 12161.
- [91] L. Vitos, A.V. Ruban, H.L. Skriver, J. Kollár, *Surf. Sci.* 411 (1998) 186.
- [92] W. Dong, G. Kresse, J. Furthmüller, J. Hafner, *Phys. Rev. B* 54 (1996) 2157.
- [93] P.A. Gravil, H. Toulhoat, *Surf. Sci.* 430 (1999) 176.
- [94] H. Ohtani, M.A. van Hove, G.A. Somorjai, *Surf. Sci.* 187 (1987) 372.
- [95] T.E. Felter, E.G. Sowa, M.A. Van Hove, *Phys. Rev. B* 40 (1989) 891.
- [96] A. Wachter, K.P. Bohnen, K.M. Ho, *Surf. Sci.* 346 (1996) 127.
- [97] S. Wilke, D. Hennig, R. Lober, M. Methfessel, M. Scheffler, *Surf. Sci.* 307/309 (1994) 76.
- [98] J. Quinn, Y.S. Li, D. Tian, H. Li, F. Jona, *Phys. Rev. B* 42 (1990) 11348.
- [99] G. Moraitis, A. Mokrani, C. Demangeat, B. M'passi-Mabiala, *Surf. Sci.* 364 (1996) 396.
- [100] V. Ledentu, W. Dong, P. Sautet, G. Kresse, J. Hafner, *Phys. Rev. B* 57 (1998) 12482.
- [101] M. Scottke, R.J. Behm, G. Ertl, V. Penka, W. Moritz, *J. Chem. Phys.* 87 (1987) 6191.
- [102] C.J. Barnes, M.Q. Ding, M. Lindroos, R.D. Diehl, D.A. Kind, *Surf. Sci.* 162 (1985) 59.
- [103] D. Tománek, S. Wilke, M. Scheffler, *Phys. Rev. Lett.* 79 (1997) 1329.
- [104] E.H. Conrad, H. Hörnis, *Prog. Surf. Sci.* 48 (1995) 221.
- [105] V.R. Dranak, G. Comelli, G. Paolucci, K.C. Prince, R. Rosei, *Surf. Sci.* 260 (1992) L24.
- [106] U. von Barth, L. Hedin, *J. Phys. C* 5 (1972) 1629.
- [107] M. Castro, *Phys. Rev. B* 43 (1991) 14378.
- [108] F. Delbecq, P. Sautet, *Phys. Rev. B* 59 (1999) 5142.
- [109] C. Barret, R. Guirado-López, D. Spanjaard, M.C. Desjonquères, A.M. Oleś, *Phys. Rev. B* 61 (2000) 7781.
- [110] N.M. Popova, L.V. Babenkova, V.N. Solnyshkova, I.G. Koh, *Zh. Fiz. Chim.* 54 (1980) 1559 (in Russian).
- [111] H. Cordatos, T. Bunluesin, R.J. Gorte, *Surf. Sci.* 323 (1995) 219.

- [112] M. Stanca, N. Dulamita, F. Buciuman, *Chemistry* 38 (1993) 153.
- [113] A.L. Cabrera, E. Morales, J.N. Armor, *J. Mater. Res.* 10 (1995) 779.
- [114] H. Conrad, G. Ertl, E.E. Latta, *Surf. Sci.* 41 (1974) 435.
- [115] R.J. Behm, V. Penka, M.G. Cattania, K. Christmann, G. Ertl, *J. Chem. Phys.* 78 (1983) 7486.
- [116] M.G. Cattania, V. Penka, R.J. Behm, K. Christmann, G. Ertl, *Surf. Sci.* 126 (1983) 382.
- [117] R. Duš, E. Nowicka, *Langmuir* 16 (2000) 584.
- [118] G. Kleinle, M. Skottke, V. Penka, G. Ertl, R.J. Behm, W. Mortiz, *Surf. Sci.* 189/190 (1987) 177.
- [119] M. Skottke, R.J. Behm, G. Ertl, V. Penka, W. Moritz, *J. Chem. Phys.* 87 (1987) 6191.
- [120] R.J. Behm, K. Christmann, G. Ertl, *Surf. Sci.* 99 (1980) 320.
- [121] T.E. Felter, R.H. Stulen, M.L. Koszykowski, G.E. Gdowski, B. Garrett, *J. Vac. Sci. Technol. A* 7 (1989) 104.
- [122] W. Lisowski, R. Duš, *Appl. Surf. Sci.* 78 (1994) 363.
- [123] D. Farias, H. Troeger, M. Patting, K.H. Rieder, *Surf. Sci.* 352/354 (1996) 155.
- [124] N. Takagi, Y. Yasui, T. Takaoka, M. Sawada, H. Yanagita, T. Aruga, M. Nishijima, *Phys. Rev. B* 53 (1996) 13767.
- [125] T. Ito, K. Umezawa, S. Nakanishi, *Shinku*, 40 (1997) 262, *Nippon Shinku Kyokai*, (quoted from *Chem. Abstr.*).
- [126] N.V. Perkas, G.D. Zakumbaeva, T.D. Levintova, *Neftekhimiya*, 35 (1995) 141 (in Russian).
- [127] I.G. Kokh, V.F. Vozdvizhenskii, L.V. Babenkova, *Zh. Fiz. Khim.* 63 (1989) 978 (in Russian).
- [128] F. Greuter, L. Strathy, E.W. Plummer, W. Eberhardt, *Phys. Rev. B: Condens. Matter* 33 (1986) 736.
- [129] V.P. Belash, I.N. Klimova, *Fiz. Met. Metalloved.* 82 (1996) 52 (in Russian).
- [130] L. Schroeter, R. David, H. Zacharias, *Surf. Sci.* 258 (1991) 259.
- [131] L. Schroeter, R. David, H. Zacharias, *J. Vac. Sci. Technol. A* 9 (1991) 1712.
- [132] L. Schroeter, R. David, H. Zacharias, *Vacuum* 41 (1990) 257.
- [133] H. Zacharias, *Appl. Phys. A* 47 (1988) 37.
- [134] H. Conrad, G. Ertl, J. Küppers, E.E. Latta, *Surf. Sci.* 58 (1976) 578.
- [135] M.V. Susic, S.V. Ribnikar, A.M. Maricic, *Int. J. Hydrogen Energy* 19 (1994) 751.
- [136] P.E.M. Seigbahn, U. Wahlgren, in: E. Shustorovich (Ed.), *Metal-Surface Reaction Energetics*, VCH Publishers, New York, 1991.
- [137] M.R.A. Blomberg, P.E.M. Seigbahn, M. Svensson, *J. Phys. Chem.* 96 (1992) 5783.
- [138] J. Massardier, J.C. Bertolini, A. Renouprez, in: *Proceedings of the 9th International Conference in Catalysis*, Calgary, Vol. 3, 1988, p. 1222.
- [139] K.R. Christmann, G. Ertl, *Surf. Sci.* 60 (1976) 365.
- [140] G.A. Somorjai, In: R.W. Jouner, R.A. van Santen (Eds.), *Elementary Reaction Steps in Heterogeneous Catalysis*, Kluwer Academic Publishers, Dordrecht, 1993, p. 3.
- [141] P. Hermann, B. Tardy, D. Simon, J.M. Guigner, B. Bigot, J.C. Bertolini, *Surf. Sci.* 307/309 (1994) 422.
- [142] J. G.Ulan, W.F. Maier, D.A. Smith, *J. Org. Chem.* 52 (1987) 3132.
- [143] D.E. White, M. Litt, *Ind. Eng. Chem. Fundam.* 14 (1975) 183.
- [144] F. Besenbacher, I. Stensgaard, K. Mortensen, *Surf. Sci.* 191 (1987) 288.
- [145] S. Castillo, A. Cruz, V. Bertin, E. Poulain, J.S. Arellano, G. Del Angel, *Int. J. Quant. Chem.* 62 (1997) 29.
- [146] I. Papai, D.R. Salahub, C. Mijoule, *Surf. Sci.* 236 (1990) 241.
- [147] A. Rochefort, J. Andzeim, N. Russo, D.R. Salahub, *J. Am. Chem. Soc.* 112 (1990) 8239.
- [148] I. Efremenko, M. Sheintuch, submitted for publication.
- [149] J.-F. Paul, P. Sautet, *Phys. Rev. B: Condens. Matter* 53 (1996) 8015.
- [150] J.-F. Paul, P. Sautet, *Surf. Sci.* 356 (1996) L403.
- [151] O.M. Løvvik, R.A. Olsen, *Phys. Rev. B* 58 (1998) 10890.
- [152] D. Tománek, Z. Sun, S.G. Louie, *Phys. Rev. B* 43 (1991) 4699.
- [153] D. Tománek, S.G. Louie, C.T. Chan, *Phys. Rev. Lett.* 57 (1986) 2594.
- [154] D. Hennig, S. Wilke, R. Löber, M. Methfessel, *Surf. Sci.* 287/288 (1993) 89.
- [155] S. Wilke, D. Hennig, R. Löber, M. Methfessel, M. Scheffler, *Surf. Sci.* 307/309 (1994) 76.
- [156] S. Wilke, D. Hennig, R. Löber, *Phys. Rev. B* 50 (1994) 2548.
- [157] A. Eichler, J. Hafner, G. Kresse, *J. Phys.: Condens. Matter* 8 (1996) 7659.
- [158] A. Eichler, J. Hafner, G. Kresse, *Surf. Rev. Lett.* 4 (1997) 1297.
- [159] W. Dong, V. Ledentu, P. Sautet, A. Eichler, J. Hafner, *Surf. Sci.* 411 (1998) 123.
- [160] W. Dong, V. Ledentu, P. Sautet, G. Kresse, J. Hafner, *Surf. Sci.* 377/379 (1997) 56.
- [161] V. Ledentu, W. Dong, P. Sautet, G. Kresse, J. Hafner, *Phys. Rev. B* 57 (1998) 12482.
- [162] R. Löber, D. Hennig, *Phys. Rev. B* 55 (1997) 4761.
- [163] W.T. Lee, L. Ford, P. Blowers, H.L. Nigg, R.I. Masel, *Surf. Sci.* 416 (1998) 141.
- [164] B.-S. Kang, K.-S. Sohn, *Phys. B: Cond. Matter* 217 (1996) 160.
- [165] E. Kampshoff, N. Waelchli, A. Menck, K. Kern, *Surf. Sci.* 360 (1996) 55.
- [166] V.R. Dhanak, G. Comelli, G. Paolucci, K.C. Prince, R. Rosei, *Surf. Sci.* 260 (1992) L24.
- [167] K. Tanaka, *Surf. Sci.* 357/358 (1996) 721.
- [168] F. Okuyama, H. Muto, H. Tsujimaki, Y. Fujimoto, *Surf. Sci.* 355 (1996) L341.
- [169] J. Yoshinobu, H. Tanaka, M. Kawai, *Phys. Rev. B* 51 (1995) 4529.
- [170] H. Niehus, C. Hiller, G. Comsa, *Surf. Sci.* 173 (1986) L599.
- [171] T.E. Felter, S.M. Foiles, M.S. Daw, R.H. Stulen, *Surf. Sci. Lett.* 171 (1986) L379.
- [172] T.E. Felter, R.H. Stulen, M.L. Koszykowski, G.E. Gdowski, B. Garrett, *J. Vac. Sci. Technol. A* 7 (1989) 104.
- [173] T.E. Felter, E.C. Sowa, M.A. Van Hove, *Phys. Rev. B* 40 (1989) 891.

- [174] G.D. Kubiak, R.H. Stulen, *J. Vac. Sci. Technol. A* 4 (1986) 1427.
- [175] W. Sesselmann, B. Woratschek, J. Küppers, G. Ertl, H. Haberland, *Phys. Rev. B* 35 (1987) 8348.
- [176] M.S. Daw, S.M. Foiles, *Phys. Rev. B* 35 (1987) 2128.
- [177] H. Ezzehar, L. Stauffer, H. Dreyse, M. Habar, *Surf. Sci.* 331/333 (A) (1995) 144.
- [178] H. Okuyama, T. Nakagawa, W. Siga, N. Takagi, M. Nishijima, T. Aruga, *J. Phys. Chem. B* 103 (1999) 7876.
- [179] H. Okuyama, T. Nakagawa, W. Siga, N. Takagi, M. Nishijima, T. Aruga, *Surf. Sci.* 411 (1998) L849.
- [180] H. Okuyama, W. Siga, N. Takagi, M. Nishijima, T. Aruga, *Surf. Sci.* 401 (1998) 344.
- [181] C. Nyberg, L. Westerlund, *Surf. Sci.* 256 (1991) 9.
- [182] H. Conrad, G. Ertl, J. Küppers, E.E. Latta, *Surf. Sci.* 58 (1976) 578.
- [183] A. Haroun, L. Stauffer, H. Dreyse, R. Riedinger, *Phys. Rev. B* 38 (1988) 12150.
- [184] M.H. Cohen, M.V. Ganduglia-Pirovano, J. Kudrnovský, *Phys. Rev. Lett.* 72 (1994) 3222.
- [185] K.D. Rendulic, G. Anger, A. Winkler, *Surf. Sci.* 208 (1989) 404.
- [186] C. Resch, H.F. Berger, K.D. Rendulic, E. Bertel, *Surf. Sci.* 316 (1994) L1105.
- [187] W.A. Diño, H. Kasai, A. Okiji, *Prog. Surf. Sci.* 63 (2000) 63.
- [188] A. Gross, M. Scheffler, *Phys. Rev. B* 57 (1998) 2493.
- [189] A. Gross, *Appl. Phys. A* 67 (1998) 627.
- [190] G.-J. Kroes, *Prog. Surf. Sci.* 60 (1999) 1–85.
- [191] J.C. Polanyi, *Science* 236 (1987) 680.
- [192] O. Novaro, C. Jarque, *Theor. Chim. Acta* 80 (1991) 19.
- [193] H. Nakatsuji, M. Hada, T. Yonezawa, *J. Am. Chem. Soc.* 109 (1987) 1902.
- [194] H. Nakatsuji, M. Hada, *J. Am. Chem. Soc.* 107 (1985) 8264.
- [195] A.A. Bagatur'yants, N.A. Anikin, G.M. Zhidomirov, V.B. Kazanskii, *Russ. J. Phys. Chem.* 55 (1981) 1157.
- [196] K. Balasubramanian, P.Y. Feng, M.Z. Liao, *J. Chem. Phys.* 88 (1988) 6955.
- [197] D. Dai, D.W. Liao, K. Balasubramanian, *J. Chem. Phys.* 102 (1995) 7530.
- [198] P.E.M. Siegban, *Theor. Chim. Acta* 87 (1994) 441.
- [199] E. Louis, F. Moscardo, E. San-Fabian, J.M. Perez-Jorda, *Phys. Rev. B* 42 (1990) 42.
- [200] W. Dong, G. Kresse, J. Hafner, *J. Mol. Catal. A* 119 (1997) 69.
- [201] W. Dong, J. Hafner, *Phys. Rev. B* 56 (1997) 15396.
- [202] A. Eichler, G. Kresse, J. Hafner, *Surf. Sci.* 397 (1998) 116.
- [203] S. Wilke, M. Scheffler, *Phys. Rev. B* 53 (1996) 4926.
- [204] V. Ledentu, W. Dong, P. Sautet, *Surf. Sci.* 412/413 (1998) 518.
- [205] A. Gross, S. Wilke, M. Scheffler, *Surf. Sci.* 357/358 (1996) 614.
- [206] A. Eichler, J. Hafner, A. Gross, M. Scheffler, *Chem. Phys. Lett.* 311 (1999) 1.
- [207] A. Eichler, J. Hafner, A. Gross, M. Scheffler, *Phys. Rev. B* 59 (1999) 13297.
- [208] M. Beutl, M. Reidler, K.D. Rendulic, *Chem. Phys. Lett.* 247 (1995) 249.
- [209] G.E. Gdowski, R.H. Stulen, T.E. Felter, *J. Vac. Sci. Technol. A* 5 (1987) 1103.
- [210] O.M. Løvvik, R.A. Olsen, *J. Chem. Phys.* 104 (1996) 4330.
- [211] R.A. Olsen, P.H.T. Philipsen, E.J. Baerends, G.J. Kroes, O.M. Løvvik, *J. Chem. Phys.* 106 (1997) 9286.
- [212] R.A. Olsen, G.J. Kroes, E.J. Baerends, *J. Chem. Phys.* 109 (1998) 2450.
- [213] R.A. Olsen, G.J. Kroes, O.M. Løvvik, E.J. Baerends, *J. Chem. Phys.* 107 (1997) 10652.
- [214] N.S. Munn, D.C. Clary, *Chem. Phys. Lett.* 266 (1997) 437.
- [215] M.L. Burke, R.J. Madix, *Surf. Sci.* 237 (1990) 1.
- [216] M. Guenin, M. Breyse, R. Frety, K. Tifouti, P. Marecot, J. Barbier, *J. Catal.* 105 (1987) 144.
- [217] P.A. Grivil, H. Toulhoat, *Surf. Sci.* 430 (1999) 192.
- [218] H.P. Toulhoat, P.A. Grivil, G. Valerio, *Book of Abstracts, in: Proceedings of the 218th ACS National Meeting on FUEL-028, American Chemical Society, New Orleans, Washington, DC, 22–26 August 1999.*
- [219] S. Speller, T. Rauch, A. Postnikov, W. Heiland, *Phys. Rev. B* 61 (2000) 7297.
- [220] S. Wilke, *Appl. Phys. A* 63 (1996) 583.
- [221] S. Wilke, M. Scheffler, *Surf. Sci.* 329 (1995) L605.
- [222] S. Wilke, M. Scheffler, *Phys. Rev. Lett.* 76 (1996) 3380.
- [223] C.M. Wei, A. Gross, M. Scheffler, *Phys. Rev. B* 57 (1998) 15572.
- [224] A. Gross, C.-M. Wei, M. Scheffler, *Surf. Sci.* 416 (1998) L1095.
- [225] A. Gross, M. Scheffler, *Phys. Rev. B* 61 (2000) 8425.
- [226] S. Wilke, M.H. Cohen, *Surf. Sci.* 380 (1997) L446.
- [227] F. Solymosi, I. Kovács, *Surf. Sci.* 260 (1992) 139.
- [228] I. Stara, V. Nehasil, V. Matolin, *Surf. Sci.* 331/333 (1995) 173.
- [229] S. Tanabe, H. Matsumoto, *J. Mater. Sci. Lett.* 13 (1994) 1540.
- [230] H. Matsumoto, S. Tanabe, *J. Phys. Chem.* 99 (1995) 6951.
- [231] M. Valden, J. Aaltonen, E. Kuusisto, M. Pessa, C.J. Barnes, *Surf. Sci.* 307/309 (1994) 193.
- [232] M. Che, C.O. Bennett, *Adv. Catal.* 36 (1989) 55.
- [233] G.D. Zakumbaeva, N.F. Toktobaeva, A.G. Kubasheva, I.G. Efremenko, *Neftekhimija*, 34 (1994) 258 (in Russian).
- [234] N.A. Zakarine, G.D. Zakumbaeva, N.F. Toktobaeva, *Electrokhimija* 19 (1983) 938 (in Russian).
- [235] N.A. Zakarine, G.D. Zakumbaeva, N.F. Toktobaeva, A.S. Kuanyshev, E.L. Litvyakova, *React. Kinet. Catal. Lett.* 26 (1984) 441.
- [236] C. Nützenadel, A. Züttel, D. Chartouni, G. Schmid, L. Schlapbach, *Eur. Phys. J. D* 8 (2000) 245–250.
- [237] I.I. Moiseev, M.N. Vargaftik, T.V. Chernysheva, T.A. Stromnova, A.E. Gekhman, G.A. Tsirkov, A.M. Makhlina, *J. Mol. Catal. A* 108 (1996) 77.
- [238] V. Oleshko, V. Volkov, W. Jacob, M. Vargaftik, I. Moiseev, G. Van Tendeloo, *Z. Phys. D* 34 (1995) 283 .
- [239] V.V. Volkov, G. Van Tendeloo, G.A. Tsirkov, N.V. Cherkashina, M.N. Vargaftik, I.I. Moiseev, V.M. Novotortsev, A.V. Kvit, A.L. Chuvilin, *J. Cryst. Growth* 163 (1996) 377.
- [240] M.N. Vargaftik, V.P. Zargorodnikov, I.P. Stolarov, I.I. Moiseev, D.I. Kochubey, V.A. Likholobov, A.L. Chuvilin, K.I. Zamarayev, *J. Mol. Catal.* 53 (1989) 315.

- [241] I.I. Moiseev, M.N. Vargaftik, *New J. Chem.* 22 (1998) 1217.
- [242] J.D. Aiken, R.G. Finke, *J. Mol. Catal. A* 145 (1999) 1.
- [243] C.R. Henry, *Surf. Sci. Rep.* 31 (1998) 325.
- [244] W. Wunderlich, Y. Ishida, R. Maurer, *Scripta metallurgica et materialia* 24 (1990) 403.
- [245] L.A. Giannuzzi, P.R. Howell, H.W. Pickering, W.R. Bitler, *Scripta metallurgica* 23 (1989) 1353.
- [246] K. Haeupl, P. Wissmann, *Thin solid films* 174 (1989) 105.
- [247] R. Herrera, M. Avalos-Borja, F. Ponce, P. Schabes-Retchkiman, D. Romeu, M. Jose-Yacamán, *Scripta metallurgica* 23 (1989) 1555.
- [248] C. Goyhenex, M. Meunier, C.R. Henry, *Surf. Sci.* 350 (1996) 103.
- [249] W.M. Straub, T. Gessmann, W. Sigle, F. Phillipp, A. Seeger, H.-E. Schaefer, *Nanostruct. Mater.* 6 (1995) 571.
- [250] R. Perez, L. Fionova, L.M. de la Garza, *Mater. Lett.* 18 (1994) 223.
- [251] A. Mehta, S.K. Malik, W.B. Yelon, *J. Magn. Magn. Mater.* 147 (1995) 309.
- [252] B. Zhang, W.A. Soffa, *IEEE Trans. Magn.* 26 (1990) 1388–1390.
- [253] W. Vogel, W.M.H. Sachtler, Z. Zhang, *Ber. Buns. Phys. Chem.* 97 (1993) 280.
- [254] M. Katagiri, M. Kubo, R. Yamauchi, A. Miyamoto, Y. Nozue, O. Terasaki, T.R. Coley, Y.S. Li, J.M. Newsam, *Jpn. J. Appl. Phys. Part 1.: Reg. Pap. Short Notes Rev. Pap.* 34 (1995) 6866.
- [255] M. Celino, G.D. Agostino, V. Rosato, *Mater. Sci. Eng. A: Struct. Mater.: Properties, Microstruct. Process.* A204 (1995) 101.
- [256] C.-L. Liu, J.B. Adams, R.W. Siegel, *Nanostruct. Mater.* 4 (1994) 265.
- [257] A. Khoutami, B. Legrand, C. Mottet, G. Tréglia, *Surf. Sci.* 307/309B (1994) 735.
- [258] C. Mottet, G. Tréglia, B. Legrand, *Surf. Sci.* 352/354 (1996) 675.
- [259] M.S. Stave, A.E. DePristo, *J. Chem. Phys.* 97 (1992) 3386.
- [260] D.R. Jennison, P.A. Schultz, M.P. Sears, *J. Chem. Phys.* 106 (1997) 1856.
- [261] Q. Cui, D.G. Musaev, K. Morokuma, *J. Chem. Phys.* 108 (1998) 8418.
- [262] Q. Cui, D.G. Musaev, K. Morokuma, *J. Phys. Chem.* 102 (1998) 6373.
- [263] J. Moc, D.G. Musaev, K. Morokuma, *J. Phys. Chem.* 104 (2000) 11606.
- [264] P.E.M. Seigbahn, *Theor. Chim. Acta* 87 (1994) 441.
- [265] I. Efremenko, E.D. German, M. Sheintuch, *J. Phys. Chem.* 104 (2000) 8089.
- [266] G. Valerio, H. Toulhoat, *J. Phys. Chem.* 100 (1996) 10827.
- [267] N. Watari, S. Ohnishi, *Phys. Rev. B* 58 (1998) 1665.
- [268] B.V. Reddy, S.N. Khanna, B.I. Dunlap, *Phys. Rev. Lett.* 70 (1993) 3323.
- [269] I. Efremenko, M. Sheintuch, *Surf. Sci.* 414 (1998) 148.
- [270] I. Efremenko, M. Sheintuch, *J. Mol. Catal. A* 160 (2000) 445.
- [271] I. Efremenko, M. Sheintuch, in press.
- [272] Y. Jinlong, F. Toigo, W. Kelin, *Phys. Rev. B* 50 (1994) 7915.
- [273] S.H. Yang, D.A. Drabold, J.B. Adams, P. Ordejon, K. Glassford, *J. Phys.: Condens. Matter* 9 (1997) L39.
- [274] F.A. Reuse, S.N. Khanna, *Chem. Phys. Lett.* 234 (1995) 77.
- [275] S.K. Nayak, B. Reddy, B.K. Rao, S.N. Khanna, P. Jena, *Chem. Phys. Lett.* 253 (1996) 390.
- [276] G. Schmid, *Nanostruct. Mater.* 6 (1995) 15.
- [277] P. Hermann, D. Simon, B. Bigot, *Surf. Sci.* 350 (1996) 301.
- [278] J.A. Alonso, *Chem. Rev.* 100 (2000) 637.
- [279] M.E. McHenry, M.A. Willard, D.E. Laughlin, *Progr. Mater. Sci.* 44 (1999) 291.
- [280] H. Dreyssé, C. Demangeat, *Surf. Sci. Rep.* 28 (1997) 65.
- [281] B. Piveteau, M.-C. Desjonqueres, A.M. Oleś, D. Spanjaard, *Surf. Sci.* 352/354 (1996) 951.
- [282] B. Piveteau, M.-C. Desjonqueres, A.M. Oleś, D. Spanjaard, *Phys. Rev. B* 53 (1996) 9251.
- [283] N. Watari, S. Ohnishi, *Phys. Rev. B* 58 (1998) 1665.
- [284] K. Lee, *Z. Phys. D* 40 (1997) 164.
- [285] K. Lee, *Phys. Rev. B* 58 (1998) 2391.
- [286] Y. Jinlong, F. Toigo, W. Kelin, *Surf. Rev. Lett.* 3 (1996) 323.
- [287] K. Balasubramanian, P.Y. Feng, M.Z. Liao, *J. Chem. Phys.* 87 (1987) 3981.
- [288] K. Balasubramanian, *J. Chem. Phys.* 89 (1988) 6310.
- [289] K. Balasubramanian, *J. Chem. Phys.* 91 (1989) 307.
- [290] D. Dai, K. Balasubramanian, *J. Chem. Phys.* 103 (1995) 648.
- [291] D. Dai, K. Balasubramanian, *Chem. Phys. Lett.* 310 (1999) 303.
- [292] H. Basch, D. Cohen, S. Topiol, *Israel J. Chem.* 19 (1980) 233.
- [293] I. Shim, K.A. Gingerich, *J. Chem. Phys.* 80 (1984) 5107.
- [294] J.M. Seminario, A.G. Zacarias, M. Castro, *Int. J. Quant. Chem.* 61 (1997) 515.
- [295] M. Neurock, R.A. van Santen, *J. Phys. Chem. B* (2000), ASAP Article published on Web.
- [296] M. Harada, H. Dexpert, *J. Phys. Chem.* 100 (1996) 565.
- [297] G.L. Estiú, M.C. Zerner, *J. Phys. Chem.* 98 (1994) 4793.
- [298] I. Efremenko, M. Sheintuch, in press.
- [299] A.M. Ferrari, C. Xiao, K.M. Neyman, G. Pacchioni, N. Rösch, *Phys. Chem. Chem. Phys.* 1 (1999) 4655.
- [300] A.J. Cox, J.G. Louderback, S.E. Apsel, L.A. Bloomfield, *Phys. Rev. B* 49 (1994) 12295.
- [301] D.C. Douglass, J.P. Bucher, L.A. Bloomfield, *Phys. Rev. B* 45 (1992) 6341.
- [302] T. Taniyama, E. Ohta, T. Sato, *Europhys. Lett.* 38 (1997) 195.
- [303] D.A. van Leeuwen, J.M. van Ruitenbeek, G. Schmid, L.J. de Jongh, *Phys. B* 194/196 (1994) 263.
- [304] Y. Volokitin, J. Sinzig, L.J. de Jongh, G. Schmid, M.N. Vargaftik, I.I. Moiseev, *Nature* 384 (1996) 621.
- [305] P. Fayet, A. Kaldor, D.M. Cox, *J. Chem. Phys.* 92 (1990) 254.
- [306] M. Neurock, *Top. Catal.* 9 (1999) 135.
- [307] V. Pallassana, M. Neurock, *Chem. Eng. Sci.* 54 (1999) 3423.
- [308] V. Pallassana, M. Neurock, G. Coulston, *Catal. Today* 50 (1999) 589.
- [309] V. Pallassana, M. Neurock, G. Coulston, *J. Phys. Chem. B* 103 (1999) 8973.

- [310] V. Pallassana, M. Neurock, *J. Phys. Chem. B* 104 (2000) 9449.
- [311] N. Watari, S. Ohnishi, Y. Ishii, *J. Phys.: Condens. Matter* 12 (2000) 6799.
- [312] C.R. Henry, *Appl. Surf. Sci.* 164 (2000) 252.
- [313] N. Tateishi, K. Yahikozawa, K. Nishimura, M. Suzuki, Y. Iwanaga, M. Watanabe, E. Enami, Y. Matsuda, Y. Takasu, *Electrochim. Acta* 36 (1991) 1235.
- [314] M.W. Lee, R.J. Wolf, J.R. Ray, *J. Alloys Comp.* 231 (1995) 343.
- [315] B. Chen, M.A. Gomez, M. Sehl, J.D. Doll, D.L. Freeman, *J. Chem. Phys.* 105 (1996) 9686.
- [316] G. Pacchioni, J. Koutecky, *J. Phys. Chem.* 91 (1987) 2658.
- [317] K. Balasubramanian, P.Y. Feng, M.Z. Liao, *J. Chem. Phys.* 87 (1987) 3981.
- [318] K. Balasubramanian, P.Y. Feng, *J. Chem. Phys.* 96 (1992) 2881.
- [319] D. Dai, K. Balasubramanian, *J. Phys. Chem.* 96 (1992) 3279.
- [320] I. Efremenko, M. Sheintuch, in press.
- [321] G. Valerio, H. Toulhoat, *J. Phys. Chem. A* 101 (1997) 1969.
- [322] P.E.M. Siegbahn, M.A. Nygren, U. Wahlgren, *NATO ASI Ser. Ser. B* 283 (1992) 267.
- [323] E.D. German, I. Efremenko, M. Sheintuch, in press.
- [324] N. Krishnankutty, M.A. Vannice, *J. Catal.* 155 (2) (1995) 312–326.
- [325] Z. Király, Á. Mastalir, F. Berger, I. Dékány, *Langmuir* 14 (1998) 1281.
- [326] A. Szűsa, F. Bergera, I. Dékány, *Colloids and Surfaces A* 174 (2000) 387.
- [327] A. Hammoudeh, J. Loboda-Cackovic, M.S. Mousa, J.H. Block, *Vacuum* 48 (1997) 187.
- [328] S.N. Reifsnnyder, M.M. Otten, H.H. Lamb, *Catal. Today* 39 (1998) 317.
- [329] J.A. Rodriguez, *Surf. Sci.* 345 (1996) 347.
- [330] F. Delbecq, P. Sautet, *Phys. Rev. B* 59 (1999) 5142.
- [331] F. Delbecq, P. Sautet, *Chem. Phys. Lett.* 302 (1999) 91.
- [332] A.L. Yakovlev, G.M. Zhidomirov, K.M. Neyman, V.A. Nasluzov, N. Roesch, *Ber. Bunsen-Ges.* 100 (1996) 413.
- [333] F. Illas, N. Lopez, J.M. Ricart, A. Clotet, J.C. Conesa, M. Fernandez-Garcia, *J. Phys. Chem. B* 102 (1998) 8017.
- [334] G. Blyholder, *J. Phys. Chem.* 68 (1964) 2772.
- [335] P. Hu, D.A. King, M.-H. Lee, M.C. Payne, *Chem. Phys. Lett.* 246 (1995) 73.
- [336] P.S. Bagus, K. Hermann, C.W. Bauschlicher Jr., *J. Chem. Phys.* 84 (1984) 1966.
- [337] P.S. Bagus, G. Pacchioni, *Surf. Sci.* 236 (1990) 233.
- [338] G. Pacchioni, F. Illas, S. Neophytides, C.G. Vayenas, *J. Phys. Chem.* 100 (1996) 16653.
- [339] F. Illas, N. López, J.M. Ricart, A. Clotet, J.C. Conesa, M. Fernandez-Garcia, *J. Phys. Chem. B* 102 (1998) 8017.
- [340] A.E. Garcia, V. Gonzalez-Robles, R. Baquero, *Phys. Rev. B* 59 (1999) 9392.
- [341] S. Zou, M.J. Weaver, *J. Phys. Chem.* 100 (1996) 4237.
- [342] S. Pick, *Phys. Rev. B* 57 (1998) 1942.
- [343] M.-S. Liao, Q.-E. Zhang, *J. Chem. Soc., Faraday Trans.* 94 (1998) 1301.
- [344] K. Wolter, O. Seifert, H. Kuhlenbeck, M. Baumer, H.-J. Freund, *Surf. Sci.* 399 (1998) 190.
- [345] B.M. Filali, C. Mijoule, N. Godbout, D.R. Salahub, *Surf. Sci.* 316 (1994) 349.
- [346] R.M. Lambert, G. Pacchioni (Eds.), *Chemisorption and Reactivity on Supported Clusters and Thin Films, Towards an Understanding of Microscopic Processes in catalysis*, in: *Proceedings of the NATO Advanced Study Institute, Erice, Trapani, Sicily, 15–26 July 1996*, Kluwer Academic Publishers, Dordrecht, 1997.
- [347] K.M. Neyman, G. Pacchioni, N. Rosch, *Recent developments and applications of modern density functional theory*, *Theor. Comput. Chem.* 4 (1996) 569–619.
- [348] J.A. Rodriguez, *Surf. Sci. Rep.* 24 (1996) 223.
- [349] N. López, G. Pacchioni, F. Maseras, F. Illas, *Chem. Phys. Lett.* 294 (1998) 611.
- [350] T. Bredow, G. Pacchioni, *Surf. Sci.* 426 (1999) 106.
- [351] B.L. Mojet, J.T. Miller, D.E. Ramaker, D.C. Koningsberger, *J. Catal.* 186 (1999) 373.
- [352] N. López, F. Illas, G. Pacchioni, *J. Am. Chem. Soc.* 121 (1999) 813.
- [353] M.J.J. Jak, C. Konstapel, A. van Kreuningen, J. Verhoeven, J.W.M. Frenken, *Surf. Sci.* 457 (2000) 295.
- [354] L. Giordano, G. Pacchioni, T. Bredow, J.F. Sanz, *Surf. Sci.* 471 (2001) 21.
- [355] C. Xu, X. Lai, G.W. Zajac, D.W. Goodman, *Phys. Rev. B* 56 (1997) 13464.
- [356] N. López, F. Illas, *J. Phys. Chem. B* 102 (1998) 1430.
- [357] K.M. Neyman, S. Vent, G. Pacchioni, N. Rösch, *IL Nuovo Cimento D* 19 (1997) 1743.
- [358] I. Yudanov, G. Pacchioni, K. Neyman, N. Rösch, *J. Phys. Chem. B* 101 (1997) 2786.
- [359] I.V. Yudanov, S. Vent, K.M. Neyman, G. Pacchioni, N. Rösch, *Chem. Phys. Lett.* 275 (1997) 245.
- [360] A.V. Matveev, K.M. Neyman, I.V. Yudanov, N. Rösch, *Surf. Sci.* 426 (1999) 123.
- [361] R. Yamauchi, I. Gunji, A. Endou, X. Yin, M. Kubo, A. Chatterjee, A. Miyamoto, *Appl. Surf. Sci.* 130/132 (1998) 572.
- [362] A.V. Matveev, K.M. Neyman, G. Pacchioni, N. Rösch, *Chem. Phys. Lett.* 299 (1999) 603.
- [363] J. Oviedo, J. Fernandez Sanz, N. López, F. Illas, *J. Phys. Chem. B* 104 (2000) 4342.
- [364] K.M. Neyman, N. Rosch, G. Pacchioni, *Appl. Catal. A* 191 (2000) 3.
- [365] A. Stirling, I. Gunji, A. Endou, Y. Oumi, M. Kubo, A. Miyamoto, *J. Chem. Soc., Faraday Trans.* 93 (1997) 1175.
- [366] B.C. Khanra, M. Menon, *Phys. B* 270 (1999) 307.
- [367] M.-F. Luo, X.-M. Zheng, *Appl. Catal. A* 189 (1999) 15.
- [368] J.M. Gatica, R.T. Baker, P. Fornasiero, S. Bernal, J. Kapar, *J. Phys. Chem. B* 105 (2001) 1191.
- [369] V.P. Zhdanov, B. Kasemo, *Surf. Sci. Rep.* 39 (2000) 25.
- [370] M. Neurock, *Top. Catal.* 9 (1999) 135.
- [371] Y. Borodko, G.A. Somorjai, *Appl. Catal. A* 186 (1999) 355.
- [372] M. Neurock, V. Pallassana, R.A. van Santen, *J. Am. Chem. Soc.* 122 (2000) 1150.

- [373] E.W. Hansen, M. Neurock, *Chem. Eng. Sci.* 54 (1999) 3411.
- [374] S.L. Kiperman, N.A. Gaidai, *Bulg. Chem. Commun.* 30 (1998) 242.
- [375] L.V. Babenkova, I.G. Kokh, N.M. Popova, *Kinet. Katal.* 27 (1986) 400.
- [376] L.V. Babenkova, I.G. Kokh, N.M. Popova, *Zh. Fiz. Khim.* 60 (1986) 3048.
- [377] I.G. Kokh, L.V. Babenkova, N.M. Popova, *React. Kinet. Catal. Lett.* 34 (1987) 243.
- [378] L.V. Babenkova, I.G. Kokh, N.M. Popova, *Kinet. Katal.* 29 (1988) 1400 (in Russian).
- [379] P.S. Cremer, G.A. Somorjai, *J. Chem. Soc., Faraday Trans.* 91 (1993) 3671.
- [380] P.S. Cremer, G.A. Somorjai, *J. Chem. Soc., Faraday Trans.* 91 (1995) 3671.
- [381] P.S. Cremer, X. Su, Y.R. Shen, G.A. Somorjai, *Catal. Lett.* 40 (1996) 143.
- [382] P.S. Cremer, X. Su, Y.R. Shen, G.A. Somorjai, *J. Am. Chem. Soc.* 118 (1996) 2942.